μ-Theraphotoxin-Pn3a inhibition of $Ca_V3.3$ channels reveals a novel isoform-selective drug binding site

Jeffrey R. McArthur[1*], Jierong Wen[2], Andrew Hung[2], Rocio K. Finol-Urdaneta[1], and David J. Adams[1]

[1] Illawarra Health and Medical Research Institute, University of Wollongong, Wollongong NSW 2522, Australia.

[2] School of Science, STEM College, RMIT University, Melbourne, VIC 3001, Australia.

*Author for correspondence:

Jeffrey R McArthur, Illawarra Health and Medical Research Institute (IHMRI)
University of Wollongong, Wollongong, NSW 2522, Australia.
Tel: +61 2 4221 5843 Email: jeffreym@uow.edu.au

Abstract

Low voltage-activated calcium currents are mediated by T-type calcium channels $Ca_V3.1$, $Ca_V3.2$, and $Ca_V3.3$, which modulate a variety of physiological processes including sleep, cardiac pace-making, pain, and epilepsy. Ca_V3 isoforms' biophysical properties, overlapping expression, and lack of subtype-selective pharmacology hinder the determination of their specific physiological roles in health and disease. We have identified μ-theraphotoxin Pn3a as the first subtype-selective spider venom peptide inhibitor of $Ca_V3.3$, with >100-fold lower potency against the other T-type isoforms. Pn3a modifies $Ca_V3.3$ gating through a depolarizing shift in the voltage dependence of activation thus decreasing $Ca_V3.3$-mediated currents in the normal range of activation potentials. Paddle chimeras of $K_V1.7$ channels bearing voltage sensor sequences from all four $Ca_V3.3$ domains revealed preferential binding of Pn3a to the S3-S4 region of domain II ($Ca_V3.3^{DII}$). This novel T-type channel pharmacological site was explored through computational docking simulations of Pn3a, site-directed mutagenesis, and full domain II swaps between Cav3 channels highlighting it as a subtype-specific pharmacophore. This research expands our understanding of T-type calcium channel pharmacology and supports the suitability of Pn3a as a molecular tool in the study of the physiological roles of $Ca_V3.3$ channels.

Introduction

Voltage-gated calcium (Ca_V) channels are activated by membrane depolarization and are involved in many physiological processes including contraction, secretion, neurotransmitter release, and gene expression (Catterall et al. 2005). In contrast to high voltage-activated (HVA) Ca^{2+} currents mediated by L-, N-, P/Q-, and R-type calcium channels that require large depolarisations, low voltage-activated (LVA) currents mediated by T-type Ca^{2+} channels are activated by small membrane depolarization and display distinctively faster activation and inactivation kinetics. T-type channel activation near resting membrane potentials generates low-threshold Ca^{2+} spikes responsible for the conspicuous burst firing and low-frequency oscillatory discharges observed in thalamic, olivary, and cerebellar neurons (Park et al. 2010, Dreyfus et al. 2010, Molineux et al. 2006, Lee et al. 2014). Thus, the biophysical properties of the T-type channels make them important regulators of cardiac and neuronal excitability (Perez-Reyes 2003, Huguenard 1996, Coulter, Huguenard, and Prince 1989) and therefore key pharmacological targets for the treatment of neurological and psychiatric disorders (Zamponi 2016, Maksemous et al. 2022).

T-type calcium channels display small single-channel conductance (T stands for transient or tiny) (Perez-Reyes et al. 1998) and are encoded by the CACNA1G ($Ca_V3.1$), CACNA1H ($Ca_V3.2$), and CACNA1I ($Ca_V3.3$) genes. The Ca_V3s have similar channel activation and inactivation kinetics and are ubiquitously expressed in the nervous, neuroendocrine, reproductive, and cardiovascular systems (Perez-Reyes 2003, Hansen 2015). In heterologous expression systems, $Ca_V3.3$-mediated currents display the slowest activation and inactivation kinetics and recover faster from inactivation (Kozlov et al. 1999), however, due to these relatively small differences, they are nearly indistinguishable from the other T-type isoform in native tissue. In the brain, abundant CACNA1I transcripts display remarkable regional distribution and appear to prevail in distal dendrites (Perez-Reyes 2003, Lee et al. 1999), where $Ca_V3.3$ currents mediate the major sleep spindle pacemaker in the thalamus (Astori et al. 2011). Transgenic mice lacking $Ca_V3.3$ channels display severe alterations to sleep-spindle generator rhythmogenic properties posing this T-type channel isoform as a critical target in the study of brain function and development (Astori et al. 2011). However, the expression of $Ca_V3.3$ channels overlaps with that of $Ca_V3.1$ and/or $Ca_V3.2$, which together with the lack of robust, isoform-selective pharmacology has hampered the elucidation of their specific contributions to cellular physiology.

T-type calcium channels share the characteristic modular topology of other voltage-gated ion channels (VGIC) (Catterall et al. 2005) that consists of a voltage sensor (VS) module formed by transmembrane segments S1 through S4 and a pore module (PM) composed of the transmembrane segments S5 and S6 connected by a re-entrant pore loop. The VS controls channel opening in response to changes in membrane potential and the PM provides aqueous passage for ions across the lipid membrane. The tetrameric arrangement of four PMs lining the permeation pathway surrounded by four VSs in either swapped or non-swapped configuration enables VGIC function (for review see (Barros et al. 2019)). In voltage-gated potassium (K_V) and transient receptor potential (TRP) channels, each monomer (1xVS + 1xPM) is encoded by a core α-subunit; whereas in voltage-gated sodium (Na_V) and Ca_V channels the α-subunit contains the four homologous, but not identical, domains (DI-DIV) joined through large intracellular linkers (Catterall 2000, Catterall et al. 2005).

Natural compounds that evolved to occlude ion channel's PM or to interact with their VS are distinguished broadly as pore blockers and gating modifiers, respectively. In VGICs, the extracellularly exposed areas of the VS are pharmacological targets of neurotoxins and synthetic compounds where at least three distinct pharmacological sites have been described in Na_V channels (Catterall et al. 2007). Within the VS is a conserved S3b-S4 paddle motif which can be transplanted into the VS of other VGICs and retain toxin sensitivity (Bosmans, Martin-Eauclaire, and Swartz 2008). α-Scorpion toxins, sea-anemone toxins, and numerous spider toxins interact with Na_V channel site 3, located in the extracellular loop between DIV-S3 and DIV-S4 thereby interfering with the conformational changes that couple channel activation to fast inactivation (Hanck and Sheets 2007). Binding of β-scorpion toxins to the S1–S2 and S3–S4 loops of domain

II (site 4) shifts the voltage dependence of channel activation towards depolarized voltages reducing the maximal current at normal activation potentials. Lastly, pharmacological site 6 (located near site 3) is targeted by the δ-conotoxins that slow Na_V channel inactivation (Terlau et al. 1996). All these gating modifier peptides (GMPs) appear to "hold" the VS in different conformations leading to their mechanism of modulation to be recognized as "voltage-sensor trapping" (Cestele et al. 1998), a phenomenon also observed in the interaction of theraphotoxins with $K_V2.1$ (Swartz and MacKinnon 1997) and agatoxins with Ca_V channels (McDonough, Mintz, and Bean 1997).

Sequence and functional conservation between the VSs lead to promiscuous interactions between peptides and small molecules across VGIC families. Examples of these include ProTx-I (*Thrixopelma pruriens,* $Na_V/K_V/Ca_V$/TRPA1) (Bladen et al. 2014, Bosmans, Martin-Eauclaire, and Swartz 2008, Gui et al. 2014, Middleton et al. 2002); ProTx-II (*Thrixopelma pruriens,* Na_V/Ca_V) (Bladen et al. 2014, Middleton et al. 2002); Kurtoxin (*Parabuthus transvaalicus,* Na_V/Ca_V) (Chuang et al. 1998); Hanatoxin (*Grammostola spatulata*, $K_V/Na_V/Ca_V$) (Bosmans, Martin-Eauclaire, and Swartz 2008, Li-Smerin and Swartz 1998, Swartz and MacKinnon 1997), and Pm1a (*Pelinobius muticus*, Na_V/K_V) (Finol-Urdaneta et al. 2022). Furthermore, small molecules such as capsaicin, capsazepine (TRPV1/K_V/Ca_V) (Caterina et al. 1997, Kuenzi and Dale 1996, McArthur, Finol-Urdaneta, and Adams 2019), and A803467 (Na_V, Ca_V) (Bladen and Zamponi 2012) amongst others are known to interact across VGIC families.

Shared ancestry and sequence conservation within the voltage sensing machinery have been used to rationalize commonalities in structure, gating kinetics, and pharmacophores between Na_V and T-type channels (Bladen and Zamponi 2012). Several Na_V-active GMPs were shown to inhibit $Ca_V3.1$ channels through interactions with the channel's domain III ($Ca_V3.1^{DIII}$) (Salari et al. 2016); whereas the potent $Na_V1.7$ inhibitor, μ-theraphotoxin Pn3a (*Pamphobeteus nigricolour*) (Deuis et al. 2017) also interacts with HVA Ca_V channels (McArthur et al. 2020).

In this study, we have used whole-cell patch clamp electrophysiology, mutagenesis, and computational docking to probe Pn3a's interactions with the LVA Ca_V3 channels. Our results support the use of Pn3a as a molecular tool for the study of $Ca_V3.3$-mediated currents in native cells and highlight a previously unrecognized pharmacophore that may enable selective targeting of T-type channel isoforms.

Results

Pn3a selectively inhibits $Ca_V3.3$ channels

Functional assessment of Pn3a activity was examined on depolarization-activated calcium currents (I_{Ca}) through the human T-type calcium channel isoforms: $Ca_V3.1$, $Ca_V3.2$, and $Ca_V3.3$. Whole-cell currents were elicited by a 100 ms test pulse to −20 mV from a holding potential (Vh) of −90 mV at a frequency of 0.2 Hz and recorded at room temperature (20-22°C, Figure 1A). Pn3a (10 μM) strongly inhibited $Ca_V3.3$-mediated currents (90.2 ± 1.9%, n = 5) with negligible effects over the two other T-type isoforms ($Ca_V3.1$: 3.8 ± 1.8%, n = 5; $Ca_V3.2$: 2.5 ± 2.5%, n = 5) (Figure 1A,B). These results indicate that Pn3a has >100-fold preference for $Ca_V3.3$ over the other highly homologous Ca_V3 isoforms. Scaled $Ca_V3.3$ macroscopic currents recorded in the absence (control) and presence of Pn3a (3 μM) display similar macroscopic activation kinetics ($\tau_{act,\ control}$ = 5.95 ± 0.54 ms vs $\tau_{act,\ Pn3a}$ = 6.37 ± 0.44 ms; P = 0.32, n = 5, paired t-test) whereas Pn3a slowed macroscopic inactivation kinetics ($\tau_{inact\ control}$ = 39.91 ± 8.25 ms vs $\tau_{inact,\ Pn3a}$ = 60.25 ± 16.02 ms; P = 0.04, n = 5, paired t-test) (representative currents provided in the inset, Figure 1A). The preferential actions of Pn3a highlight its potential as a molecular probe to isolate and study the contribution of $Ca_V3.3$ currents in native cells.

Pn3a inhibitory potency against $Ca_V3.3$ currents was assessed at increasing peptide concentrations from which a concentration-response curve was built (Figure 1C). Fit to a standard Hill equation rendered an IC_{50} value of 0.96 ± 0.05 μM (*nH* 0.87 ± 0.04, n = 5 per concentration) for the inhibition of $Ca_V3.3$ channels. This Hill coefficient is consistent with a 1:1 stoichiometry between Pn3a toxin and $Ca_V3.3$ channels.

The change in $Ca_V3.3$ peak current amplitude during Pn3a *washin* and *washout* enables the assessment of Pn3a binding to $Ca_V3.3$ channels. The inhibition of $Ca_V3.3$ calcium currents by Pn3a was mono-exponential with progressively faster time constants (τ_{obs}) at increasing peptide concentration (Figure 1D). The on- and off-rate constants (k_{on} and k_{off}) were determined from the fit to the linear plot of $1/\tau_{obs}$ versus [Pn3a] (Figure 1D, n = 5 per concentration), where k_{on} is the slope and k_{off} is the y-intercept. The linear regression line results in a k_{on} of 0.036 $\mu M^{-1}sec^{-1}$ and k_{off} of 0.052 sec^{-1} which yield a K_D of 1.4 μM, in close agreement with the IC_{50} value obtained (Figure 1C). k_{off} was confirmed by fitting the *washout* to a single exponential (k_{off} = 0.055 ± 0.002 sec^{-1}). Hence, Pn3a inhibits $Ca_V3.3$-mediated currents without apparent actions on $Ca_V3.1$ or $Ca_V3.2$ exposed to up to 10 μM peptide.

Pn3a modifies the gating of $Ca_V3.3$

The voltage dependence of $Ca_V3.3$ activation, deactivation, inactivation and recovery from inactivation were investigated in the absence and presence of Pn3a (3 μM) (Figure 2 and Table 1). $Ca_V3.3$ activation is shifted ~13 mV to more depolarized potentials (control $V_{0.5}$= −28.3 ± 0.4 mV, n = 5, vs Pn3a $V_{0.5}$ = −15.3 ± 0.4 mV, n = 5; P<0.0001), indicating that a stronger depolarization is required to enable channel opening in the presence of Pn3a (Figure 2A,C). The voltage dependence of $Ca_V3.3$ steady-state inactivation (SSI) was not affected by exposure to the spider peptide (control $V_{0.5}$= −56.3 ± 0.3 mV, n = 5, vs Pn3a $V_{0.5}$ = −56.6 ± 0.4 mV, n = 5, P = 0.57, Figure 2B-C). Consistent with the observed slowing of inactivation, $Ca_V3.3$-mediated currents inactivated by a 200 ms pre-pulse to –20 mV recovered faster in the presence of Pn3a (τ = 0.22 ± 0.01 s, n = 5) than under control conditions (τ = 0.34 ± 0.01 s, n = 5; P < 0.0001) (Figure 2D-E) suggesting a potential Pn3a-dependent destabilization of the inactivated state.

The voltage dependence of Pn3a inhibition of I_{Ca} and Na^+ mediated (I_{Na}) $Ca_V3.3$ currents was examined at various test potentials (Figure 3A and Figure 3-figure supplement 1). Pn3A displayed a decrease in $Ca_V3.3$ I_{Ca} inhibition at more depolarized potentials consistent with Pn3a preferentially binding to the down-state of the voltage sensor. To examine the voltage dependence across a larger voltage range, extracellular Ca^{2+} was removed permitting Na^+ to be the primary charge carrier through the open $Ca_V3.3$. Similar to that seen for I_{Ca}, I_{Na} showed a similar voltage dependence, with stronger inhibition at more negative potentials (Figure 3-figure supplement 1).

The time course of tail current decay reflects the rate of channels leaving the open state (test potential) and entering the closed state (deactivation) upon return to the holding potential. We examined the modulation of $Ca_V3.3$ channel deactivation through tail current kinetic analysis. Pn3a-modified $Ca_V3.3$ currents displayed a faster deactivation time constant ($\tau_{deactivation}$) across all potentials tested compared to control (Figure 3 B-C). This data suggests that Pn3a binding may destabilize the open state or stabilize the closed one. These results that Pn3a is a $Ca_V3.3$ gating modifier peptide that decreases channel availability by increasing the energy required for channel opening.

Pn3a interacts with $Ca_V3.3^{DII}$ S3-S4 paddles

To ascertain Pn3a's pharmacophore on $Ca_V3.3$ channels, we applied the chimeric approach of transplanting its four S3-S4 paddles into a voltage-gated potassium channel based on a similar template to that previously described for $K_V2.1/Ca_V3.1$ chimeras (Salari et al. 2016). We substituted portions of the S3b-S4 from $Ca_V3.3$ DI to DIV into the $K_V1.7$ channel backbone. The sequence alignment of $Ca_V3.3$ DI-DIV S3-S4 segments and the corresponding extracellular region of $K_V1.7$ is presented in Figure 4A.

All four $K_V1.7/Ca_V3.3$ chimeric constructs were functional, mediating large K^+ currents that displayed distinct gating properties from those of the parental wild-type $K_V1.7$ ($V_{0.5}$ = −10.5 ± 0.6 mV, n = 7; Figure 4B, inset). Briefly, chimeric $K_V1.7/Ca_V3.3^{DI}$, $K_V1.7/Ca_V3.3^{DII}$ and $K_V1.7/Ca_V3.3^{DIII}$ displayed 80-100 mV depolarizing shifts in channel activation ($K_V1.7/Ca_V3.3^{DI}$ $V_{0.5}$ = 91.3 ± 0.4 mV, n = 5; $K_V1.7/Ca_V3.3^{DII}$ $V_{0.5}$ = 97.3 ± 0.4 mV, n = 9; $K_V1.7/Ca_V3.3^{DIII}$ $V_{0.5}$ = 71.3 ± 0.8 mV, n = 7, two-way ANOVA, P < 0.05), whereas $K_V1.7/Ca_V3.3^{DIV}$ activation was ~50 mV hyperpolarized ($K_V1.7/Ca_V3.3^{DIV}$ $V_{0.5}$ = −60.8 ± 0.8 mV, n = 5; two-way ANOVA, P < 0.05) (Figure 4). Our results

are in broad agreement with previous reports for $Ca_V3.1$, where DIV displays a hyperpolarizing shift and DI-III show a variable depolarizing shift in $V_{0.5}$ (Salari et al. 2016).

$K_V1.7/Ca_V3.3^{DI-IV}$ chimeras and the parental $K_V1.7$ construct were analysed in control and after exposure to Pn3a (1 μM) and representative currents (Vh = −100 mV, with test pulse to +40 mV ($K_V1.7$), +120 mV ($K_V1.7/Ca_V3.3^{DI-III}$) or 0 mV ($K_V1.7/Ca_V3.3^{DIV}$)) in both conditions are included as insets (Fig 5). Similar to the parental channel, peak currents of $K_V1.7/Ca_V3.3^{DI}$ and $K_V1.7/Ca_V3.3^{DIV}$ chimaeras were insensitive to Pn3a ($K_V1.7$: 1.0 ± 0.8%, n = 6; $Ca_V3.3^{DI}$: 0.6 ± 0.5%, n = 5, and $Ca_V3.3^{DIV}$: 0.4 ± 0.2%, n = 5) (Figure 5A, D, E), with $K_V1.7/Ca_V3.3^{DIII}$ displaying modest peptide-dependent inhibition (12.0 ± 0.6%, n = 6) (Figure 5C).

In contrast, currents mediated by $K_V1.7/Ca_V3.3^{DII}$ were significantly reduced (54.2 ± 2.9%, n = 7) in the presence of Pn3a (Figure 5B). Furthermore, conductance-voltage relationships for each S3-S4 paddle chimera in the absence and presence of Pn3a were built from peak currents in response to standard I-V protocols ($K_V1.7$ -60 to +90 mV; $K_V1.7/Ca_V3.3^{DI-III}$ 0 to +160 mV; and $K_V1.7/Ca_V3.3^{DIV}$ −120 to +30 mV; Vh = −100 mV, 0.2 Hz). The latter analysis revealed a ~15 mV rightward shift in the half voltage of activation ($V_{0.5}$) exclusively in the $Ca_V3.3^{DII}$ chimera when exposed to Pn3a (control $V_{0.5}$ = 97.3 ± 0.4 mV, n = 9; vs Pn3a $V_{0.5}$ = 112.6 ± 0.4 mV, n = 7, $p < 0.0001$), strongly suggesting that Pn3a interacts with the S3-S4 region of domain II in $Ca_V3.3$.These results suggest that the positive shift in activation $V_{0.5}$ observed in the full length and DII chimera likely underpins Pn3a's mechanism of $Ca_V3.3$ inhibition, highlighting the differences in pharmacological properties of each voltage-sensing module.

Molecular determinants of Pn3a inhibition of $Ca_V3.3$

The critical role of DII was further supported by examining the effects of Pn3a on full-length Cav3 channel constructs where the whole DII was swapped between isoforms. Replacement of $Ca_V3.3^{DII}$ with either $Ca_V3.1^{DII}$ or $Ca_V3.2^{DII}$ resulted in partial (Cav3.3/$Ca_V3.1^{DII}$: 33 ± 4.1%, n = 5, one-way ANOVA $P < 0.0001$) or complete (Cav3.3/$Ca_V3.2^{DII}$: 2.2 ± 1.5%, n = 5, one-way ANOVA $P < 0.0001$) loss of inhibition compared to the full length $Ca_V3.3$ (90.2 ± 1.9% n = 5) in the presence of 10 μM Pn3a (Figure 6E). The reverse constructs where $Ca_V3.3^{DII}$ was grafted onto $Ca_V3.1$ ($Ca_V3.1/Ca_V3.3^{DII}$) or $Ca_V3.2$ ($Ca_V3.2/Ca_V3.3^{DII}$) afforded Pn3a-sensitivity to the parental Cav3 channel such that currents mediated by $Ca_V3.1/Ca_V3.3^{DII}$ were inhibited by 71.4 ± 4.1% (n = 5), and $Ca_V3.2/Ca_V3.3^{DII}$ by 68.0 ± 3.6 % (n=5) (Fig. 6F). Thus, verifying that $Cav3.3^{DII}$ is required for Pn3a interaction with T-type calcium channels.

Molecular docking was used to assess the most energetically favoured binding poses for Pn3a on the extracellular-facing pockets of DII of the three channel isoforms, $Ca_V3.3$, $Ca_V3.2$, and $Ca_V3.1$ (Figure 6 and Figure 6-figure supplement 1, 2 and 3). Comparative analyses of toxin interactions with the other T-type calcium channel members showed that Pn3a forms fewer contacts with the DII S3-S4 linker of $Ca_V3.1$ and $Ca_V3.2$, compared to $Ca_V3.3$ (Figure 6D). Evaluation of the inter-residue contacts between the docked Pn3a and $Ca_V3.3^{DII}$ revealed several receptor residues predicted to form close contacts with the toxin (Fig. 6D, upper left inset). In particular, Pn3a-K17 is predicted to be in close proximity to D689 and may form an especially strong interaction due to the possibility of a salt bridge contact. Guided by the docking results, point mutations of selected $Cav3.3^{DII}$ amino acids (E628A, Q687A, D689A, R696A, K1294A, N1310A, and Q1362A) were explored within full-length Cav3.3 channels. In comparison to wild type Cav3.3, $Ca_V3.3$-D689A (27.6 ± 1.8%, n = 5, one-way ANOVA $P < 0.0001$) and $Ca_V3.3$-E628A (68.2 ± 2.0%, n = 5, one-way ANOVA $P < 0.0001$) displayed significant reductions in Pn3a inhibition (Fig. 6F), whereas the peptide activity in the other mutants studied ($Ca_V3.3$-Q687A: 83.6 ± 0.5%, n = 5; $Ca_V3.3$-R696A: 83.6 ± 2.7%, n = 5; $Ca_V3.3$-K1294A: 84.8 ± 1.2%, n = 5; $Ca_V3.3$-N1310A 79.2 ± 3.5%, n = 5; and $Ca_V3.3$-Q1362A 85.4 ± 1.3%, n = 5) was unaffected. The relevance of Cav3.3-D689 interaction with Pn3a was further substantiated by the loss of inhibition in the analogous charge neutralization Kv1.7/$Cav3.3^{DII}$ chimeric construct Kv1.7/$Cav3.3^{DII}$-D262A (Figure 5-figure supplement 1), thus pinpointing key molecular determinants responsible for Pn3a's selective inhibition of $Ca_V3.3$.

Discussion

The present study demonstrates the functional activity of Pn3a as a gating modifier inhibitor of human $Ca_V3.3$ channels with >100-fold higher activity over $Ca_V3.1$ and $Ca_V3.2$. Our chimeric approaches revealed Pn3a's preference for $Ca_V3.3^{DII}$ S3-S4 paddle region, whereas comparative molecular docking amongst isoforms identified a novel binding site putatively determining Pn3a's proclivity towards $Ca_V3.3$. Thus, this investigation highlights Pn3a as the first molecular probe available for the study of $Ca_V3.3$ contribution in native cells. We propose that the unique features of Pn3a's $Ca_V3.3$-specificity may be exploited to design isoform-selective T-type calcium channel modulators.

Ca_V3 sub-type selectivity

μ-Theraphotoxin-Pn3a was originally described as a potent $Na_V1.7$ inhibitor with an IC_{50} of 0.9 nM, while also inhibiting other tetrodotoxin (TTX)-sensitive Na_V channels ($Na_V1.1$-1.4 and $Na_V1.6$) with 10- to 100-fold less potency (Deuis et al. 2017). More recently Pn3a was shown to inhibit murine dorsal root ganglion HVA calcium currents and human $Ca_V1.2$, $Ca_V1.3$, $Ca_V2.1$ and $Ca_V2.2$ calcium channels expressed in HEK293T cells (IC_{50} 3-10 μM) (McArthur et al. 2020). Perhaps a more interesting aspect of Pn3a activity is its >100-fold selectivity for human $Ca_V3.3$ over both $Ca_V3.1$ and $Ca_V3.2$ (Figure 1) which distinguishes this spider peptide as a unique isoform-selective modulator of T-type calcium channels. Only a handful of venom-derived peptides have been shown to interact with T-type calcium channels. The scorpion peptide Kurtoxin was the first GMP reported to modulate Ca_V3 channels with a high affinity for $Ca_V3.1$ and $Ca_V3.2$ channels (Chuang et al. 1998). The closely related peptide KLI, from *Parabuthus granulatus*, was later shown to inhibit $Ca_V3.3$ with an IC_{50} ~450 nM (Olamendi-Portugal et al. 2002). However, the T-type isoform selectivity and binding site of these two peptides were not comprehensively documented at the time. The activity of spider Protoxins I and II against the three Ca_V3 channels revealed that ProTx-I preferentially modulates $Ca_V3.1$ channels whereas ProTx-II targets $Ca_V3.2$ (Bladen et al. 2014, Salari et al. 2016). Thus, Pn3a complements the molecular toolbox for the study of T-type calcium channels in native tissues.

Voltage dependence and current kinetics

Pn3a inhibits $Ca_V3.3$ by inducing a depolarizing shift in $Ca_V3.3$ voltage dependence of activation in a manner analogous to Kurtoxin, Protoxin I, and Protoxin II actions on $Ca_V3.1$ channels (Edgerton, Blumenthal, and Hanck 2010, Chuang et al. 1998). This is also consistent with Pn3a's modulation of $Na_V1.7$ (Deuis et al. 2017) but not of $Ca_V2.2$ channels for which a hyperpolarizing shift in the voltage dependence of inactivation was associated with current inhibition (McArthur et al. 2020). In contrast to the 2-fold slower recovery from inactivation reported for Pn3a-bound $Na_V1.7$ channels, currents mediated by Pn3a-modified $Ca_V3.3$ channels recover ~1.5-fold faster from inactivation (Figure 2D/E). This, and the observed slowing of inactivation (at high Po), are suggestive of a toxin-induced destabilization of the inactivated state. Nevertheless, given Pn3a's voltage dependence of Cav3.3 inhibition (Figure 3A), voltage-dependent unbinding of the toxin at more positive potentials could also contribute to an apparent faster recovery from inactivation as reported for Ca_V active toxins such as AgaIVA (McDonough et al. 1997) and SNX482 (Bourinet et al. 2001).

Pn3a inhibition of $Ca_V3.3$ was voltage-dependent with greater inhibition at more negative potentials (Figure 3A) similar to Kurtoxin-inhibited $Ca_V3.1$ channel currents (Chuang et al. 1998). However, a delay in $Ca_V3.1$ activation kinetics was apparent in the presence of both Kurtoxin and ProTx-II (Edgerton, Blumenthal, and Hanck 2010, Chuang et al. 1998) but not in Pn3a-modified $Ca_V3.3$. The spider peptides Pn3a (this study) and ProTx-II (Edgerton, Blumenthal, and Hanck 2010) appear to slow T-type channel deactivation suggestive of stabilization of the channel's closed state, whereas Kurtoxin, from scorpion venom, does not affect $Ca_V3.1$ channel closure (Chuang et al. 1998) highlighting incompletely understood aspects of GMP/VGIC interactions.

Interaction of Pn3a with $Ca_V3.3$ VS paddles

The portability of the S3-S4 paddle region was shown more than 20 years ago (Swartz and MacKinnon 1997). To date, most studies, if not all, have used the $K_V2.1$ channel backbone for the identification of GMPs binding sites in voltage-gated sodium and calcium channels expressed in *Xenopus* oocytes (Bosmans, Martin-Eauclaire, and Swartz 2008, Salari et al. 2016). For our chimera studies, we selected the $K_V1.7$ backbone given the remarkable scarcity of GMPs interacting with K_V1 channels (Finol-Urdaneta et al. 2020). The robust expression of this channel in heterologous systems (Finol-Urdaneta, Struver, and Terlau 2006, Finol-Urdaneta et al. 2012) and resistance to Pn3a modulation (Figure 5E/F) make it suitable to assess peptide binding to $Ca_V3.3$ paddle motifs in mammalian cells. The generated $K_V1.7/Ca_V3.3$ constructs resulted in four functional, voltage-gated chimeric potassium channels that exhibited distinct gating properties to those of the parental scaffold reflecting the acquisition of the grafted S3-S4 paddle regions from DI-DIV of $Ca_V3.3$. Namely, $K_V1.7/Ca_V3.3^{DI\text{-}DIII}$ all displayed >80 mV depolarizing shifts in channel activation compared to wild-type $K_V1.7$, whereas the $Ca_V3.3^{DIV}$ bearing chimeric construct presented a comparable magnitude shift in the hyperpolarizing direction (Fig 4).

Analogous chimeric approaches of $K_V2.1/Ca_V3.1D^{I\text{-}IV}$ have indicated that ProTx-II, PaTx-1, GsAF-I, and GsAF-II exert their inhibitory actions predominantly through interaction with $Ca_V3.1^{DIII}$ (Salari et al. 2016), whereas Pn3a does so by targeting $K_V2.1/Na_V1.7^{DII}$ and $K_V2.1/Na_V1.7^{DIV}$ (Deuis et al. 2017). Here we observe modest Pn3a inhibition of $K_V1.7/Ca_V3.3^{DIII}$ mediated currents and potent effects on $K_V1.7/Ca_V3.3^{DII}$ chimeras with current inhibition coupled to toxin-induced rightward shift in the voltage dependence of activation as evidence of preferential interactions with $Ca_V3.3^{DII}$ (Figure 5B/F). A substantial body of literature has shown that DI-DIII and DIV are important for Na_V activation and inactivation, respectively (Ahern et al. 2016). Thus, the predominant effects of Pn3a on $Ca_V3.3$ activation are consistent with its interaction with DII of this channel.

Furthermore, it has been shown that ProTx-I inhibits $Ca_V3.3/Ca_V3.1^{DIV}$ chimeric channels while interacting less potently with $Ca_V3.3/Ca_V3.1^{DII}$. However, a clear binding site could not be delineated through mutation of individual $Ca_V3.1^{DII}$ residues as those did not result in measurable changes in toxin affinity (Bladen et al. 2014). Our domain swap experiments verified that Pn3a's actions are largely determined by $Cav3.3^{DII}$ from which aspartate in position 689 constitutes an important interaction site as shown by its alanine replacement in Cav3.3 and $Kv1.7/Cav3.3^{DII}$. It can be surmised that subtle, but significant GMP/VGIC interaction differences highlight incompletely understood idiosyncrasies related to molecular aspects of ion channel function between isoforms as well as how peptide interactions may be affected by the experimental manipulation and conditions used for their study.

A novel binding site with Ca_V3 sub-type selectivity

Our molecular docking calculations suggest that Pn3a binds within the groove formed between extracellular linkers S1-S2 and S3-S4 supported by electrostatic interactions with the $Ca_V3.3^{DII}$ S3-S4 paddle, which bears some similarity with the $Ca_V3.1$/ProTx-II complex in which favourable binding sites occur in $Ca_V3.1$'s DII and DIV (Bladen et al. 2014).

The interaction of Pn3a with $Ca_V3.3$ channels involves substantial interactions within the S3-S4 paddle (K17-Q687) and S4 (H18-R696) of $Ca_V3.3^{DII}$, while a close contact may also exist between the sidechain of D689 and the sidechain of Pn3a-K17 (Figure 6D, upper left panel). The latter is consistent with the establishment of a salt bridge between these residues. The loss of Pn3a inhibition upon charge neutralization at this position lends support to this docking model.

The proximity between cationic residues (K17 and H18) on loop 3 of Pn3a and the $Ca_V3.3D^{II}$ S3-S4 paddle places this peptide at the hollow between S1-S2 and S3-S4 linkers in a binding conformation similar to other tarantula toxins targeting Na_V channel site 4, like HwTX-IV, ProTx-II and HNTX-III, that bear critical basic and hydrophobic amino acids within loop 4 that interact with acidic residues on the Na_V^{DII}'s S3-S4 linker (Deng et al. 2013, Liu et al. 2013, Bosmans and Swartz 2010) (Figure 6-figure supplement 1 and 2). Hence the predicted Pn3a interaction with $Ca_V3.3$ appears to share overall similarities with previously identified spider peptide toxins modulating Na_V and K_V channels in which the common bioactive surface consists of positively charged and hydrophobic residues (Smith et al. 2007, Corzo et al. 2005).

The findings presented here establish Pn3a as a gating modifier modulator of $Ca_V3.3$ channels interacting with the paddle motif of DII's voltage sensor module through putative stabilization of the closed/resting state and concomitant channel current inhibition. Pn3a's >100-fold higher potency against $Ca_V3.3$ over the other two Ca_V3 isoforms is rationalized through recognition of a previously unknown drug binding site that may be exploited in the design of isoform-selective Ca_V3 channel modulators.

Materials and Methods

Cell lines, culture and transfections

Human embryonic kidney (HEK293T, authenticated by STR profiling and mycoplasm free) cells containing the SV40 Large T-antigen were cultured and transfected by calcium phosphate method as reported previously (McArthur et al. 2018). In brief, cells were cultured at 37ºC, 5% CO2 in Dulbecco's Modified Eagle's Medium (DMEM, Invitrogen Life Technologies, VIC, Australia), supplemented with 10% fetal bovine serum (FBS, Bovigen, VIC, Australia), 1% GlutaMAX and penicillin-streptomycin (Invitrogen). HEK293T cells were then transiently co-transfected with the different voltage-gated calcium channel isoforms and green fluorescent protein (GFP) for visualization, using the calcium phosphate method. cDNAs encoding human $Ca_V3.1$ (provided by Dr. G. Zamponi), human $Ca_V3.2$ (a1Ha-pcDNA3 was a gift from Dr. E. Perez-Reyes, Addgene #45809 (Cribbs et al. 1998), human $Ca_V3.3$ (a1Ic-HE3-pcDNA3 also from Dr. E. Perez-Reyes, Addgene #45810 (Gomora et al. 2002) in combination with green fluorescent protein. $Cav3^{DII}$ swap constructs and $K_V1.7/Ca_V3.3$ chimeras were custom synthesized by GeneScript, NJ, USA.

Chinese Hamster Ovary (CHO) cells were used to express $K_V1.7$ and $K_V1.7$-$Ca_V3.3$ paddle chimeras. Cell culture conditions were the same as the HEK293T cells except DMEM was substituted with DMEM/F12 (Invitrogen). CHO cells were transfected with cDNAs encoding $K_V1.7$ and $K_V1.7/Ca_V3.3^{DI\text{-}DIV}$ chimeras using Lipofectamine 2000 (Invitrogen) as per the manufacturer's protocol and used for recordings 12-48 hr post-transfection.

Electrophysiology

Whole-cell patch clamp configuration was used to record calcium (I_{Ca}) or potassium (I_K) currents in transiently transfected HEK293T cells. Recordings were made using a MultiClamp 700B amplifier, digitized with a DigiData1440, and controlled using Clampex11.1 software (Molecular Devices, CA, USA). Whole-cell currents were sampled at 100 kHz and then filtered to 10 kHz, with leak and capacitive currents subtracted using a −P/4 protocol for Ca^{2+} currents and uncorrected for K^+ currents. All recordings were series compensated 60-80%. External solution for I_{Ca} contained in mM: 100 NaCl, 10 $CaCl_2$, 1 $MgCl_2$, 5 CsCl, 30 TEA-Cl, 10 D-glucose and 10 HEPES, pH 7.3 with TEA-OH. External solution for I_K contained in mM: 140 NaCl, 5 KCl, 1 $MgCl_2$, 2 $CaCl_2$, 10 Glucose, and 10 HEPES, pH 7.3 with NaOH. Fire-polished borosilicate (1B150F-4, World Precision Instruments, FL, USA) patch pipettes were used with resistance of 1-3 MΩ. Intracellular recording solution contained as follows (mM): 140 KGluconate, 5 NaCl, 2 $MgCl_2$, 5 EGTA, and 10 HEPES, pH 7.2 with KOH. Cells were continuously perfused with extracellular solution at a rate of 1.2 ml/min, while toxin application was superfused onto the cell through a capillary tube attached to a syringe pump (2 µl/min), directly onto the cell being recorded. Synthetic µ-Theraphotoxin Pn3a was kindly provided by the Vetter laboratory (Institute of Molecular Bioscience, University of Queensland) and reconstituted in ddH_2O.

For experiments on Ca_V3s, all cells were held at −90 mV. To examine the onset of block, test pulses (100 ms, 0.5 Hz) to −20 mV were applied. To generate activation curves, cells were pulsed from −90 to +40 mV in 10 mV increments at 0.5 Hz. SSI curves were generated by measuring the peak current from a test pulse to −20 mV when preceded by a 1 s pre-pulse from −90 to 20 mV (0.1 Hz). Recovery from inactivation curves was produced by varying the time (0-2 sec) between two depolarizing pules to −20 mV (P1 200 ms, P2 50 ms).

For experiments on $K_V1.7$ and $Ca_V3.3$ DI-IV chimeras, cells were held at –80 mV and activation curves were generated by applying a 50 ms pre-pulse to varying potentials depending on the channel construct examined ($K_V1.7$ –60 to 90 mV, DI-III 0 to +160 mV, and DIV –120 to +30 mV) followed by a 50 ms test pulse to measure tail currents ($K_V1.7$ 0 mV, DI-III +80 mV, and DIV –20 mV). To measure the onset of Pn3a inhibition, test pulses (50 ms) from a holding potential of –100 mV to a test potential determined for each channel construct ($K_V1.7$ 40 mV, DI-III 120 mV, and DIV 0 mV) were elicited at 0.2 Hz.

Structures and homology modelling of Human T-type calcium channels and the docking of Pn3a

The cryo-EM structures of human $Ca_V3.1$ (PDB ID: 6KZO) (Zhao et al. 2019) and $Ca_V3.3$ (PDB ID: 7WLI) (He et al. 2022) were used for docking calculations. The comparative model of human$Ca_V3.2$ was built upon the Cryo-EM structure of h$Ca_V3.1$ in the apo form (PDB ID: 6KZO) via SWISS-MODEL server (*swissmodel*.expasy.org). The 3-D structure of μ-theraphotoxin (TRTX)-Pn3a (PDB ID: 5T4R) (Deuis et al. 2017) was docked into the *three* T-type calcium channels via Autodock Vina with a grid box of 40Å × 40Å × 40Å. We also compared the binding mode and the binding affinity among the four VSs of $Ca_V3.3$, to identify which VS module Pn3a preferentially targets. The docking results were further analysed via Discovery studio 2017R2 and visualized in visual molecular dynamics (VMD) (Humphrey, Dalke, and Schulten 1996).

Data and statistical analysis

All data analysis and graphs were generated in OriginPro (Origin Lab Corporation, MA, USA). Concentration-response curves were generated by plotting peak current amplitudes in the presence of Pn3a (I_{Pn3a}), over the current before Pn3a application ($I_{Control}$). The resulting curve was fit with a sigmoidal curve according to the following expression:

$$(1)\ I_{Pn3a}/I_{Control} = 1 + [Pn3a]^n/(IC50^n + [Pn3a]^n)$$

Where IC50 is the half-maximal inhibitory concentration and n is the Hill coefficient. Activation (2) and SSI (3) curves were fit by the modified Boltzmann equation:

$$(2)\ I = 1 - 1/(1 + \exp\left(\frac{Vm - V_{0.5}}{ka}\right)) \qquad (3)\ G = 1/(1 + \exp\left(\frac{Vm - V_{0.5}}{ka}\right))$$

Where I is the current or G is the conductance, Vm is the pre-pulse potential, $V_{0.5}$ is the half-maximal activation potential and ka is the slope factor. Recovery from inactivation plots were fit using a single exponential of the following equation:

$$(4)\ \left(\frac{P2}{P1}\right) = 1 + A_{fast} * \exp\left(-\frac{t}{t}\right)$$

where τ is the time constant and *A* is the amplitude. Statistical significance ($p < 0.05$) was determined using paired or unpaired t-test or 2-way ANOVA followed by a Tukey multiple comparison test if F achieves the level of statistical significance of $P < 0.05$ and no variance inhomogeneity. All data are presented as mean ± SEM (n), where n is individual cells with all experimental results containing $n \geq 5$ individual cells.

Acknowledgments

This work was supported by the Rebecca Cooper Foundation for Medical Research Project Grant [PG2019396] to J.R.M and the National Health and Medical Research Council (NHMRC) Program Grant [APP1072113] to D.J.A. J.R.M and R.K.F-U are grateful to Emma and Zack O. Yepugas for continuous support. Computational resources were provided by the National Computational Infrastructure (NCI) which is funded by the Australian Government, and the Pawsey Supercomputing Centre which is funded by the Australian Government and the

Government of Western Australia. We acknowledge PRACE for awarding access to the Piz Daint cluster at the Swiss National Supercomputing Centre (CSCS), Switzerland.

Competing Interests

The authors declare no conflict of interest.

461 **References**

462 Ahern, C. A., J. Payandeh, F. Bosmans, and B. Chanda. 2016. "The hitchhiker's guide to the
463 voltage-gated sodium channel galaxy." *J Gen Physiol* 147 (1):1-24. doi:
464 10.1085/jgp.201511492.
465 Astori, S., R. D. Wimmer, H. M. Prosser, C. Corti, M. Corsi, N. Liaudet, A. Volterra, P. Franken, J. P.
466 Adelman, and A. Luthi. 2011. "The Ca(V)3.3 calcium channel is the major sleep spindle
467 pacemaker in thalamus." *Proc Natl Acad Sci U S A* 108 (33):13823-8. doi:
468 10.1073/pnas.1105115108.
469 Barros, F., L. A. Pardo, P. Dominguez, L. M. Sierra, and P. de la Pena. 2019. "New Structures and
470 Gating of Voltage-Dependent Potassium (Kv) Channels and Their Relatives: A Multi-
471 Domain and Dynamic Question." *Int J Mol Sci* 20 (2). doi: 10.3390/ijms20020248.
472 Bladen, C., J. Hamid, I. A. Souza, and G. W. Zamponi. 2014. "Block of T-type calcium channels by
473 protoxins I and II." *Mol Brain* 7:36. doi: 10.1186/1756-6606-7-36.
474 Bladen, C., and G. W. Zamponi. 2012. "Common mechanisms of drug interactions with sodium
475 and T-type calcium channels." *Mol Pharmacol* 82 (3):481-7. doi:
476 10.1124/mol.112.079715.
477 Bosmans, F., M. F. Martin-Eauclaire, and K. J. Swartz. 2008. "Deconstructing voltage sensor
478 function and pharmacology in sodium channels." *Nature* 456 (7219):202-8. doi:
479 10.1038/nature07473.
480 Bosmans, F., and K. J. Swartz. 2010. "Targeting voltage sensors in sodium channels with spider
481 toxins." *Trends in pharmacological sciences* 31 (4):175-182. doi:
482 10.1016/j.tips.2009.12.007.
483 Bourinet, E., S. C. Stotz, R. L. Spaetgens, G. Dayanithi, J. Lemos, J. Nargeot, and G. W. Zamponi.
484 2001. "Interaction of SNX482 with domains III and IV inhibits activation gating of
485 alpha(1E) (Ca(V)2.3) calcium channels." *Biophys J* 81 (1):79-88. doi: 10.1016/S0006-
486 3495(01)75681-0.
487 Caterina, M. J., M. A. Schumacher, M. Tominaga, T. A. Rosen, J. D. Levine, and D. Julius. 1997.
488 "The capsaicin receptor: a heat-activated ion channel in the pain pathway." *Nature* 389
489 (6653):816-24. doi: 10.1038/39807.
490 Catterall, W. A. 2000. "From ionic currents to molecular mechanisms: the structure and function
491 of voltage-gated sodium channels." *Neuron* 26 (1):13-25. doi: 10.1016/s0896-
492 6273(00)81133-2.
493 Catterall, W. A., S. Cestele, V. Yarov-Yarovoy, F. H. Yu, K. Konoki, and T. Scheuer. 2007. "Voltage-
494 gated ion channels and gating modifier toxins." *Toxicon* 49 (2):124-41. doi:
495 10.1016/j.toxicon.2006.09.022.
496 Catterall, W. A., E. Perez-Reyes, T. P. Snutch, and J. Striessnig. 2005. "International Union of
497 Pharmacology. XLVIII. Nomenclature and structure-function relationships of voltage-
498 gated calcium channels." *Pharmacol Rev* 57 (4):411-25. doi: 10.1124/pr.57.4.5.
499 Cestele, S., Y. Qu, J. C. Rogers, H. Rochat, T. Scheuer, and W. A. Catterall. 1998. "Voltage sensor-
500 trapping: enhanced activation of sodium channels by beta-scorpion toxin bound to the
501 S3-S4 loop in domain II." *Neuron* 21 (4):919-31. doi: 10.1016/s0896-6273(00)80606-6.
502 Chuang, R. S., H. Jaffe, L. Cribbs, E. Perez-Reyes, and K. J. Swartz. 1998. "Inhibition of T-type
503 voltage-gated calcium channels by a new scorpion toxin." *Nat Neurosci* 1 (8):668-74.
504 doi: 10.1038/3669.
505 Corzo, G., P. Escoubas, E. Villegas, I. Karbat, D. Gordon, M. Gurevitz, T. Nakajima, and N. Gilles.
506 2005. "A spider toxin that induces a typical effect of scorpion α-toxins but competes

with β-toxins on binding to insect sodium channels." *Biochemistry* 44 (5):1542-1549. doi: 10.1021/bi048434k.

Coulter, D. A., J. R. Huguenard, and D. A. Prince. 1989. "Calcium currents in rat thalamocortical relay neurones: kinetic properties of the transient, low-threshold current." *J Physiol* 414:587-604. doi: 10.1113/jphysiol.1989.sp017705.

Cribbs, L. L., J. H. Lee, J. Yang, J. Satin, Y. Zhang, A. Daud, J. Barclay, M. P. Williamson, M. Fox, M. Rees, and E. Perez-Reyes. 1998. "Cloning and characterization of alpha1H from human heart, a member of the T-type Ca2+ channel gene family." *Circ Res* 83 (1):103-9. doi: 10.1161/01.res.83.1.103.

Deng, M., X. Luo, L. Jiang, H. Chen, J. Wang, H. He, and S. Liang. 2013. "Synthesis and biological characterization of synthetic analogs of Huwentoxin-IV (Mu-theraphotoxin-Hh2a), a neuronal tetrodotoxin-sensitive sodium channel inhibitor." *Toxicon* 71:57-65. doi: 10.1016/j.toxicon.2013.05.015.

Deuis, J. R., Z. Dekan, J. S. Wingerd, J. J. Smith, N. R. Munasinghe, R. F. Bhola, W. L. Imlach, V. Herzig, D. A. Armstrong, K. J. Rosengren, F. Bosmans, S. G. Waxman, S. D. Dib-Hajj, P. Escoubas, M. S. Minett, M. J. Christie, G. F. King, P. F. Alewood, R. J. Lewis, J. N. Wood, and I. Vetter. 2017. "Pharmacological characterisation of the highly NaV1.7 selective spider venom peptide Pn3a." *Sci Rep* 7:40883. doi: 10.1038/srep40883.

Dreyfus, F. M., A. Tscherter, A. C. Errington, J. J. Renger, H. S. Shin, V. N. Uebele, V. Crunelli, R. C. Lambert, and N. Leresche. 2010. "Selective T-type calcium channel block in thalamic neurons reveals channel redundancy and physiological impact of I(T)window." *J Neurosci* 30 (1):99-109. doi: 10.1523/JNEUROSCI.4305-09.2010.

Edgerton, G. B., K. M. Blumenthal, and D. A. Hanck. 2010. "Inhibition of the activation pathway of the T-type calcium channel Ca(V)3.1 by ProTxII." *Toxicon* 56 (4):624-36. doi: 10.1016/j.toxicon.2010.06.009.

Finol-Urdaneta, R. K., A. Belovanovic, M. Micic-Vicovac, G. K. Kinsella, J. R. McArthur, and A. Al-Sabi. 2020. "Marine Toxins Targeting Kv1 Channels: Pharmacological Tools and Therapeutic Scaffolds." *Mar Drugs* 18 (3). doi: 10.3390/md18030173.

Finol-Urdaneta, R. K., M. S. Remedi, W. Raasch, S. Becker, R. B. Clark, N. Struver, E. Pavlov, C. G. Nichols, R. J. French, and H. Terlau. 2012. "Block of Kv1.7 potassium currents increases glucose-stimulated insulin secretion." *EMBO Mol Med* 4 (5):424-34. doi: 10.1002/emmm.201200218.

Finol-Urdaneta, R. K., N. Struver, and H. Terlau. 2006. "Molecular and Functional Differences between Heart mKv1.7 Channel Isoforms." *J Gen Physiol* 128 (1):133-45. doi: 10.1085/jgp.200609498.

Finol-Urdaneta, R. K., R. Ziegman, Z. Dekan, J. R. McArthur, S. Heitmann, K. Luna-Ramirez, H. S. Tae, A. Mueller, H. Starobova, Y. K. Chin, J. S. Wingerd, E. A. B. Undheim, B. Cristofori-Armstrong, A. P. Hill, V. Herzig, G. F. King, I. Vetter, L. D. Rash, D. J. Adams, and P. F. Alewood. 2022. "Multitarget nociceptor sensitization by a promiscuous peptide from the venom of the King Baboon spider." *Proc Natl Acad Sci U S A* 119 (5). doi: 10.1073/pnas.2110932119.

Gomora, J. C., J. Murbartian, J. M. Arias, J. H. Lee, and E. Perez-Reyes. 2002. "Cloning and expression of the human T-type channel Ca(v)3.3: insights into prepulse facilitation." *Biophys J* 83 (1):229-41. doi: 10.1016/s0006-3495(02)75164-3.

Gui, J., B. Liu, G. Cao, A. M. Lipchik, M. Perez, Z. Dekan, M. Mobli, N. L. Daly, P. F. Alewood, L. L. Parker, G. F. King, Y. Zhou, S. E. Jordt, and M. N. Nitabach. 2014. "A tarantula-venom

553 peptide antagonizes the TRPA1 nociceptor ion channel by binding to the S1-S4 gating
554 domain." *Curr Biol* 24 (5):473-83. doi: 10.1016/j.cub.2014.01.013.
555 Hanck, D. A., and M. F. Sheets. 2007. "Site-3 toxins and cardiac sodium channels." *Toxicon* 49
556 (2):181-93. doi: 10.1016/j.toxicon.2006.09.017.
557 Hansen, P. B. 2015. "Functional importance of T-type voltage-gated calcium channels in the
558 cardiovascular and renal system: news from the world of knockout mice." *Am J Physiol*
559 *Regul Integr Comp Physiol* 308 (4):R227-37. doi: 10.1152/ajpregu.00276.2014.
560 He, L., Z. Yu, Z. Geng, Z. Huang, C. Zhang, Y. Dong, Y. Gao, Y. Wang, Q. Chen, L. Sun, X. Ma, B.
561 Huang, X. Wang, and Y. Zhao. 2022. "Structure, gating, and pharmacology of human
562 CaV3.3 channel." *Nat Commun* 13 (1):2084. doi: 10.1038/s41467-022-29728-0.
563 Huguenard, J. R. 1996. "Low-threshold calcium currents in central nervous system neurons."
564 *Annu Rev Physiol* 58:329-48. doi: 10.1146/annurev.ph.58.030196.001553.
565 Humphrey, W., A. Dalke, and K. Schulten. 1996. "VMD: visual molecular dynamics." *J Mol Graph*
566 14 (1):33-8, 27-8. doi: 10.1016/0263-7855(96)00018-5.
567 Kozlov, A. S., F. McKenna, J. H. Lee, L. L. Cribbs, E. Perez-Reyes, A. Feltz, and R. C. Lambert. 1999.
568 "Distinct kinetics of cloned T-type Ca2 + channels lead to differential Ca2 + entry and
569 frequency-dependence during mock action potentials." *Eur J Neurosci* 11 (12):4149-58.
570 doi: 10.1046/j.1460-9568.1999.00841.x.
571 Kuenzi, F. M., and N. Dale. 1996. "Effect of capsaicin and analogues on potassium and calcium
572 currents and vanilloid receptors in Xenopus embryo spinal neurones." *Br J Pharmacol*
573 119 (1):81-90. doi: 10.1111/j.1476-5381.1996.tb15680.x.
574 Lee, J. H., A. N. Daud, L. L. Cribbs, A. E. Lacerda, A. Pereverzev, U. Klockner, T. Schneider, and E.
575 Perez-Reyes. 1999. "Cloning and expression of a novel member of the low voltage-
576 activated T-type calcium channel family." *J Neurosci* 19 (6):1912-21.
577 Lee, S. E., J. Lee, C. Latchoumane, B. Lee, S. J. Oh, Z. A. Saud, C. Park, N. Sun, E. Cheong, C. C.
578 Chen, E. J. Choi, C. J. Lee, and H. S. Shin. 2014. "Rebound burst firing in the reticular
579 thalamus is not essential for pharmacological absence seizures in mice." *Proc Natl Acad*
580 *Sci U S A* 111 (32):11828-33. doi: 10.1073/pnas.1408609111.
581 Li-Smerin, Y., and K. J. Swartz. 1998. "Gating modifier toxins reveal a conserved structural motif
582 in voltage-gated Ca2+ and K+ channels." *Proc Natl Acad Sci U S A* 95 (15):8585-9. doi:
583 10.1073/pnas.95.15.8585.
584 Liu, Z., T. Cai, Q. Zhu, M. Deng, J. Li, X. Zhou, F. Zhang, D. Li, J. Li, Y. Liu, W. Hu, and S. Liang. 2013.
585 "Structure and function of hainantoxin-III, a selective antagonist of neuronal
586 tetrodotoxin-sensitive voltage-gated sodium channels isolated from the Chinese bird
587 spider Ornithoctonus hainana." *The Journal of biological chemistry* 288 (28):20392-
588 20403. doi: 10.1074/jbc.M112.426627.
589 Maksemous, N., C. D. Blayney, H. G. Sutherland, R. A. Smith, R. A. Lea, K. N. Tran, O. Ibrahim, J.
590 R. McArthur, L. M. Haupt, Z. Cader, R. K. Finol-Urdaneta, D. J. Adams, and L. R. Griffiths.
591 2022. "Investigation of CACNA1I Cav3.3 Dysfunction in Hemiplegic Migraine Abbreviated
592 title: CACNA1I variants in hemiplegic migraine." *Front Mol Neurosci*. doi:
593 10.3389/fnmol.2022.892820.
594 McArthur, J. R., R. K. Finol-Urdaneta, and D. J. Adams. 2019. "Analgesic transient receptor
595 potential vanilloid-1-active compounds inhibit native and recombinant T-type calcium
596 channels." *Br J Pharmacol* 176 (13):2264-2278. doi: 10.1111/bph.14676.
597 McArthur, J. R., L. Motin, E. C. Gleeson, S. Spiller, R. J. Lewis, P. J. Duggan, K. L. Tuck, and D. J.
598 Adams. 2018. "Inhibition of human N- and T-type calcium channels by an ortho-

599 phenoxyanilide derivative, MONIRO-1." *Br J Pharmacol* 175 (12):2284-2295. doi:
600 10.1111/bph.13910.
601 McArthur, J. R., N. R. Munasinghe, R. K. Finol-Urdaneta, D. J. Adams, and M. J. Christie. 2020.
602 "Spider Venom Peptide Pn3a Inhibition of Primary Afferent High Voltage-Activated
603 Calcium Channels." *Front Pharmacol* 11:633679. doi: 10.3389/fphar.2020.633679.
604 McDonough, S. I., R. A. Lampe, R. A. Keith, and B. P. Bean. 1997. "Voltage-dependent inhibition
605 of N- and P-type calcium channels by the peptide toxin omega-grammotoxin-SIA." *Mol*
606 *Pharmacol* 52 (6):1095-104. doi: 10.1124/mol.52.6.1095.
607 McDonough, S. I., I. M. Mintz, and B. P. Bean. 1997. "Alteration of P-type calcium channel gating
608 by the spider toxin omega-Aga-IVA." *Biophys J* 72 (5):2117-28. doi: 10.1016/S0006-
609 3495(97)78854-4.
610 Middleton, R. E., V. A. Warren, R. L. Kraus, J. C. Hwang, C. J. Liu, G. Dai, R. M. Brochu, M. G.
611 Kohler, Y. D. Gao, V. M. Garsky, M. J. Bogusky, J. T. Mehl, C. J. Cohen, and M. M. Smith.
612 2002. "Two tarantula peptides inhibit activation of multiple sodium channels."
613 *Biochemistry* 41 (50):14734-47. doi: 10.1021/bi026546a.
614 Molineux, M. L., J. E. McRory, B. E. McKay, J. Hamid, W. H. Mehaffey, R. Rehak, T. P. Snutch, G.
615 W. Zamponi, and R. W. Turner. 2006. "Specific T-type calcium channel isoforms are
616 associated with distinct burst phenotypes in deep cerebellar nuclear neurons." *Proc*
617 *Natl Acad Sci U S A* 103 (14):5555-60. doi: 10.1073/pnas.0601261103.
618 Olamendi-Portugal, T., B. I. Garcia, I. Lopez-Gonzalez, J. Van Der Walt, K. Dyason, C. Ulens, J.
619 Tytgat, R. Felix, A. Darszon, and L. D. Possani. 2002. "Two new scorpion toxins that
620 target voltage-gated Ca2+ and Na+ channels." *Biochem Biophys Res Commun* 299
621 (4):562-8. doi: 10.1016/s0006-291x(02)02706-7.
622 Park, Y. G., H. Y. Park, C. J. Lee, S. Choi, S. Jo, H. Choi, Y. H. Kim, H. S. Shin, R. R. Llinas, and D.
623 Kim. 2010. "Ca(V)3.1 is a tremor rhythm pacemaker in the inferior olive." *Proc Natl*
624 *Acad Sci U S A* 107 (23):10731-6. doi: 10.1073/pnas.1002995107.
625 Perez-Reyes, E. 2003. "Molecular physiology of low-voltage-activated t-type calcium channels."
626 *Physiol Rev* 83 (1):117-61. doi: 10.1152/physrev.00018.2002.
627 Perez-Reyes, E., L. L. Cribbs, A. Daud, A. E. Lacerda, J. Barclay, M. P. Williamson, M. Fox, M. Rees,
628 and J. H. Lee. 1998. "Molecular characterization of a neuronal low-voltage-activated T-
629 type calcium channel." *Nature* 391 (6670):896-900. doi: 10.1038/36110.
630 Salari, A., B. S. Vega, L. S. Milescu, and M. Milescu. 2016. "Molecular Interactions between
631 Tarantula Toxins and Low-Voltage-Activated Calcium Channels." *Sci Rep* 6:23894. doi:
632 10.1038/srep23894.
633 Smith, J. J., T. R. Cummins, S. Alphy, and K. M. Blumenthal. 2007. "Molecular interactions of the
634 gating modifier toxin ProTx-II with Nav1.5: implied existence of a novel toxin binding site
635 coupled to activation." *Journal of Biological Chemistry* 282 (17):12687-12697. doi:
636 10.1074/jbc.M610462200.
637 Swartz, K. J., and R. MacKinnon. 1997. "Mapping the receptor site for hanatoxin, a gating
638 modifier of voltage-dependent K+ channels." *Neuron* 18 (4):675-82. doi:
639 10.1016/s0896-6273(00)80307-4.
640 Terlau, H., K. J. Shon, M. Grilley, M. Stocker, W. Stuhmer, and B. M. Olivera. 1996. "Strategy for
641 rapid immobilization of prey by a fish-hunting marine snail." *Nature* 381 (6578):148-51.
642 doi: 10.1038/381148a0.
643 Zamponi, G. W. 2016. "Targeting voltage-gated calcium channels in neurological and psychiatric
644 diseases." *Nat Rev Drug Discov* 15 (1):19-34. doi: 10.1038/nrd.2015.5.

645 Zhao, Y., G. Huang, Q. Wu, K. Wu, R. Li, J. Lei, X. Pan, and N. Yan. 2019. "Cryo-EM structures of
646 apo and antagonist-bound human Cav3.1." *Nature* 576 (7787):492-497. doi:
647 10.1038/s41586-019-1801-3.

648

649 **Figure Legends**
650
651 **Figure 1. Pn3a preferentially inhibits human $Ca_V3.3$-mediated Ca^{2+} currents. (A)** $Ca_V3.3$
652 (left), $Ca_V3.1$ (middle), and $Ca_V3.2$ (right) currents elicited by 100 ms step depolarization to –20
653 mV (Vh –90 mV, 0.2 Hz) in the absence (control, black) and presence of 3 μM Pn3a (pink). Scale
654 bars: 0.2 nA, 20 ms. The inset shows scaled $Ca_V3.3$ currents in control and in the presence of
655 Pn3a with similar kinetics. **(B)** Bar graph summarizing % inhibition by 10 μM Pn3a of the three
656 Ca_V3 isoforms. **(C)** Concentration-response curve for Pn3a inhibition of $Ca_V3.3$ currents. **(D)**
657 Kinetics of Pn3a inhibition of $Ca_V3.3$. K_{obs} was determined at three concentrations and fit with a
658 linear equation where $K_{obs} = k_{on} \cdot [Pn3a] + k_{off}$.

659 **Figure 2. Pn3a produces a depolarizing shift in the voltage dependence of activation and**
660 **speeds up recovery from inactivation of $Ca_V3.3$. (A-C)** Effect of Pn3a on the voltage
661 dependence of $Ca_V3.3$. Representative currents from **(A)** activation or **(B)** steady-state
662 inactivation protocols, in the absence (Top: Control, Black) and presence of 3 μM Pn3a (middle:
663 Pn3a, pink) using the standard protocols (bottom). Scale bars: 0.5 nA, 10 ms. **(C)** Activation
664 (circles) and steady-state inactivation (squares) relationships for $Ca_V3.3$ in the absence (black)
665 and presence of 3 μM Pn3a (pink). Dashed lines represent non-normalized activation and
666 inactivation curves of Pn3a **(D)** Representative recovery from inactivation currents in control (left)
667 and presence of 3 μM Pn3a (right) (trace shown in blue highlights the current recovered after 0.3
668 s). Scale bars: 0.2 nA, 200 ms. **(E)** Recovery from inactivation in the absence (black) and
669 presence of 3 μM Pn3a (pink).

670 **Figure 2-figure supplement 1.** Current-Voltage relation of control (black) and 3 μM Pn3a (pink)
671 inhibition of human $Ca_V3.3$.

Figure 3. Pn3a inhibition of $Ca_V3.3$ is stronger at hyperpolarized potentials and speeds up channel deactivation. (A) Voltage dependence of Pn3a inhibition of $Ca_V3.3$-mediated Ca^{2+} currents. **(B)** Representative $Ca_V3.3$ tail currents at different voltages in the absence (black) and presence (pink) of 3 μM Pn3a. **(C)** Summary of the time constant (τ) of $Ca_V3.3$ deactivation upon return to the holding potential (–90 mV) plotted against the activating (pre-pulse) potential in the absence (control, black) and the presence of Pn3a (3 μM, pink).

Figure 3-figure supplement 1. Voltage dependence of Pn3a inhibition of human $Ca_V3.3$ when Na^+ is the charge carrier. **(A)** Representative traces showing the inhibition by 3 μM Pn3a of inward and outward I_{Na} through $Ca_V3.3$ at −30, 0, 30, and 60 mV. Scale bars: 1 nA, 20 ms. **(B)** Graph showing % inhibition of I_{Na} by 3 μM Pn3a from −40 to +60 mV.

Figure 4. Chimeric constructs of the $K_V1.7$ channel with the $Ca_V3.3$ voltage sensor paddles. (A) Sequence alignment between paddle regions of $Ca_V3.3$ and $K_V1.7$. The coloured bolded sequences from $Ca_V3.3$ DI (yellow), $Ca_V3.3$ DII (pink), $Ca_V3.3$ DIII (blue), and $Ca_V3.3$ DIV (green) were grafted onto $K_V1.7$ (black). **(B)** Representative current traces in response to 50 ms long I-V protocols used to evaluate the voltage dependence of activation of all constructs (Vh = –80 mV). $K_V1.7/Ca_V3.3^{DI}$ (0 to 160 mV), $K_V1.7/Ca_V3.3^{DII}$ (0 to 160 mV), $K_V1.7/Ca_V3.3^{DIII}$ (0 to 160 mV) and $K_V1.7/Ca_V3.3^{DIV}$ (–120 to 30 mV). The traces highlighted in colour correspond to currents near half-activation potential ($V_{0.5}$). **(C)** Activation curves for all chimeras: $K_V1.7/Ca_V3.3^{DI}$ (yellow), $K_V1.7/Ca_V3.3^{DII}$ (pink), $K_V1.7/Ca_V3.3^{DIII}$ (blue), and $K_V1.7/Ca_V3.3^{DIV}$ (green) and the parental channel $K_V1.7$ (black). The dotted line corresponds to $Ca_V3.3$ activation for reference. The inset contains representative $K_V1.7$ currents (–60 to 90 mV). All scale bars: 1 nA, 10 ms.

Figure 5. Pn3a shifts the activation of $K_V1.7/Ca_V3.3^{DII}$ chimeric channels. G/G_{max}-V relationships and representative currents obtained in the absence (control, black) and presence of 1 μM Pn3a (pink) for **(A)** $K_V1.7/Ca_V3.3^{DI}$ (90 mV), **(B)** $K_V1.7/Ca_V3.3^{DII}$ (100 mV), **(C)** $K_V1.7/Ca_V3.3^{DIII}$ (70 mV), and **(D)** $K_V1.7/Ca_V3.3^{DIV}$ (–60 mV). **(E)** Bar graph showing percent inhibition by 1 μM Pn3a of $K_V1.7/Ca_V3.3^{DI-IV}$ chimeras and $K_V1.7$ wt. **(F)** $K_V1.7$ G/G_{max}-V relationship and current traces obtained in the absence (control) and presence of Pn3a (-10 mV).

Figure 5-figure supplement 1. Bar graph showing percent inhibition by 1 μM Pn3a of $K_V1.7/Ca_V3.3^{DII}$ chimera and mutants $K_V1.7/Ca_V3.3^{DII}$-Q260A, $K_V1.7/Ca_V3.3^{DII}$-D262A, and $K_V1.7/Ca_V3.3^{DII}$-R269A (corresponding to Cav3.3 -Q687A, -D689A, and -R696A, respectively).

Figure 6. Pn3a and $Ca_V3.3$ interactions and subtype specificity. (**A**) Top view of Pn3a (magenta) binding to $Cav3.3^{DII}$. The S3 (lime), S3-4 loop (ice blue), and S4 (pink) are highlighted. (**B**) Side view of the binding conformation of Pn3a to $Ca_V3.3^{DII}$. (**C**) Left: Pn3a amino acid sequence and disulfide connectivity. Right: 3-D structure of Pn3a (PDB ID: 5T4R (Deuis et al. 2017)) showing cysteine residues in CPK linked by salt bridges (yellow). **(D)** Pairwise amino acid interactions between Pn3a (magenta) with the extracellular loop of $Ca_V3.3^{DII}$ (top left, blue), $Ca_V3.2^{DII}$ (top right, yellow), and $Ca_V3.1^{DII}$ (bottom left, purple). Overlap of the Pn3a-bound ribbon structures of all Cav3 highlighting differences in extracellular S3-S4 loops between $Ca_V3.3$ and the other two Ca_V3 isoforms (bottom right). S1, S1-2 loop, and S2 were removed for clarity. **(E)** Bar graph showing percent inhibition by 10 μM Pn3a of Ca_V3^{DII} domain-swapped Cav3 constructs and point mutants.

713 **Figure 6-figure supplement 1.** The binding conformation of Pn3a at voltage-sensing domain
714 (VSD)-II of T-type calcium channels. The interactive residues of the spider toxin contacting with
715 corresponding residues of the VSDII of $Ca_V3.3$ (A), $Ca_V3.2$ (B), and $Ca_V3.1$ (C), respectively. For
716 clarity, the binding domain of Ca_V3 channel shown in transparent color was removed after rotating
717 the binding conformation around the y-axis by 180º (in the bottom). The coloring method in VMD
718 was adopted for the residues and surfaces, demonstrating non-polar (white), basic (blue), acidic
719 (red) and polar (green) residues.

720 **Figure 6-figure supplement 2.** Minor interactions between the residues of Pn3a and the
721 corresponding residues on hCa_V3 channels.

722 **Figure 6-figure supplement 3.** Predicted binding affinity values for Pn3a binding to the DI, DII,
723 DIII and DIV domains of the VS modules on $hCa_V3.3$ calculated using Autodock Vina.

724

725

Table 1. Activation and inactivation values of $Ca_V3.3$ and Kv1.7-$Ca_V3.3^{DI-IV}$ chimers in the absence (control) and presence of Pn3a (3 μM for $Ca_V3.3$; 1 μM for $K_V1.7$-$Ca_V3.3^{D1-IV}$ chimeras). * Significant determined from paired t-test with significance threshold set to P < 0.05.

		Control	***Pn3a***
hCa$_V$3.3	***V$_{0.5}$ Activation***	–28.3 ± 0.4 mV (5)	**–15.3 ± 0.4 mV (5) ***
	ka Slope factor	7.5 ± 0.3 (5)	**10.0 ± 0.3 (5) ***
	V$_{0.5}$ SSI	–56.3 ± 0.3 mV (5)	–56.6 ± 0.4 mV (5)
	ka Slope factor	7.5 ± 0.2 (5)	8.4 ± 0.4 (5)
	τ Recovery	0.34 ± 0.01 ms (5)	**0.22 ± 0.01 (5) ***
K$_V$1.7	***V$_{0.5}$ Activation***	–10.5 ± 0.6 mV (7)	-
	ka Slope factor	9.9 ± 0.5 (7)	-
K$_V$1.7-Ca$_V$3.3^{DI}	***V$_{0.5}$ Activation***	91.3 ± 0.4 mV (5)	88.2 ± 0.3 mV (5)
	ka Slope factor	1.0 ± 0.3 (5)	11.8 ± 0.2 (5)
K$_V$1.7-Ca$_V$3.3^{DII}	***V$_{0.5}$ Activation***	97.3 ± 0.4 mV (9)	**112.6 ± 0.4 mV (7) ***
	ka Slope factor	14.1 ± 0.3 (9)	**12.3 ± 0.4 (7) ***
K$_V$1.7-Ca$_V$3.3^{DIII}	***V$_{0.5}$ Activation***	71.3 ± 0.8 mV (7)	74.7 ± 0.9 mV (5)
	ka Slope factor	21.1 ± 0.7 (7)	22.0 ± 0.8 (5)
K$_V$1.7-Ca$_V$3.3^{DIV}	***V$_{0.5}$ Activation***	–60.8 ± 0.8 mV (5)	–60.8 ± 0.4 mV (5)
	ka Slope factor	10.1 ± 0.7 (5)	10.0 ± 0.4 (5)

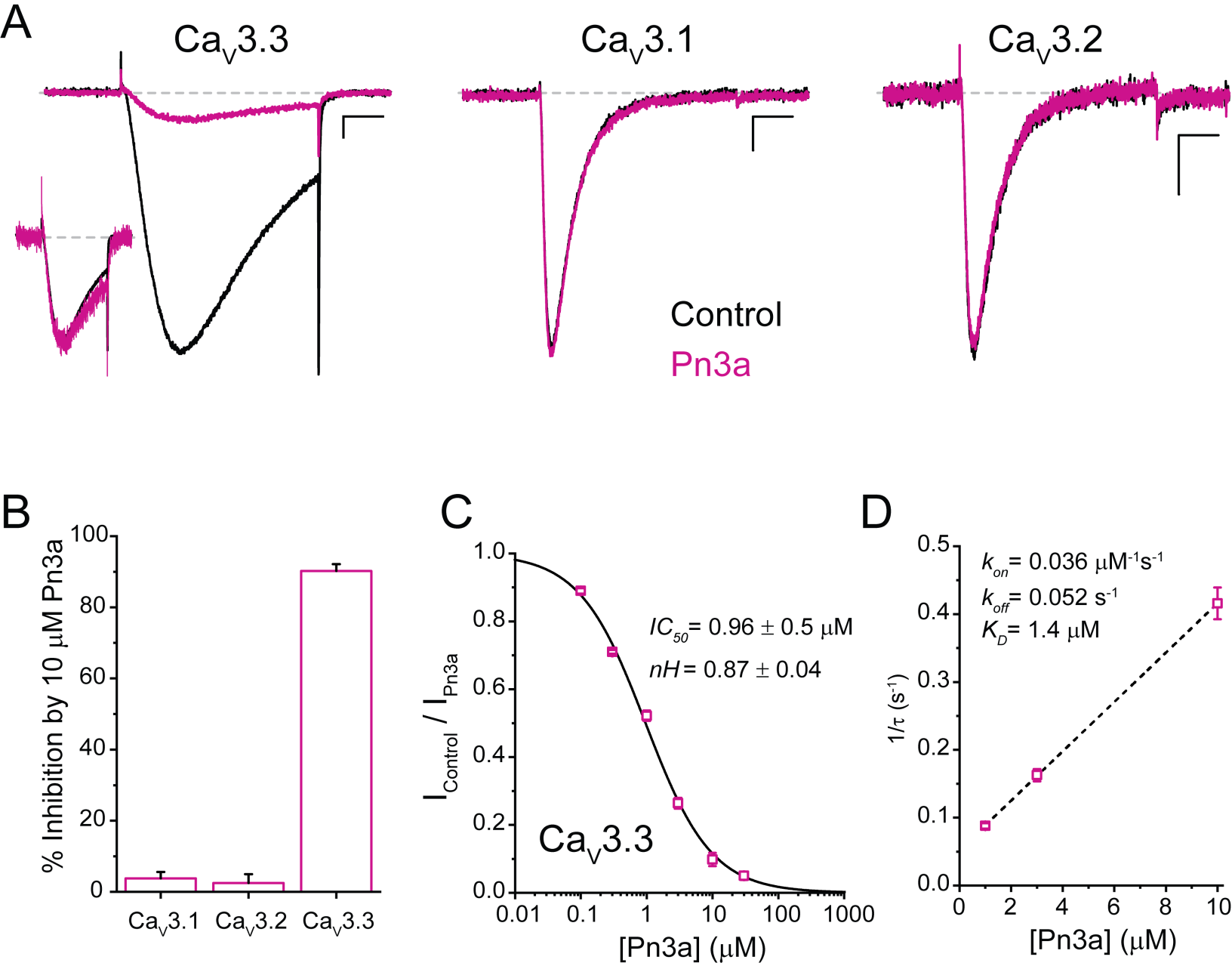
A
$Ca_V3.3$
$Ca_V3.1$
$Ca_V3.2$
Control
Pn3a
B
% Inhibition by 10 μM Pn3a
100
80
60
40
20
0
$Ca_V3.1$
$Ca_V3.2$
$Ca_V3.3$
C
$I_{Control} / I_{Pn3a}$
1.0
0.8
0.6
0.4
0.2
0.0
IC_{50}= 0.96 ± 0.5 μM
nH = 0.87 ± 0.04
$Ca_V3.3$
0.01
0.1
1
10
100
1000
[Pn3a] (μM)
D
1/τ (s^{-1})
0.5
0.4
0.3
0.2
0.1
0.0
k_{on}= 0.036 $\mu M^{-1}s^{-1}$
k_{off}= 0.052 s^{-1}
K_D= 1.4 μM
0
2
4
6
8
10
[Pn3a] (μM)

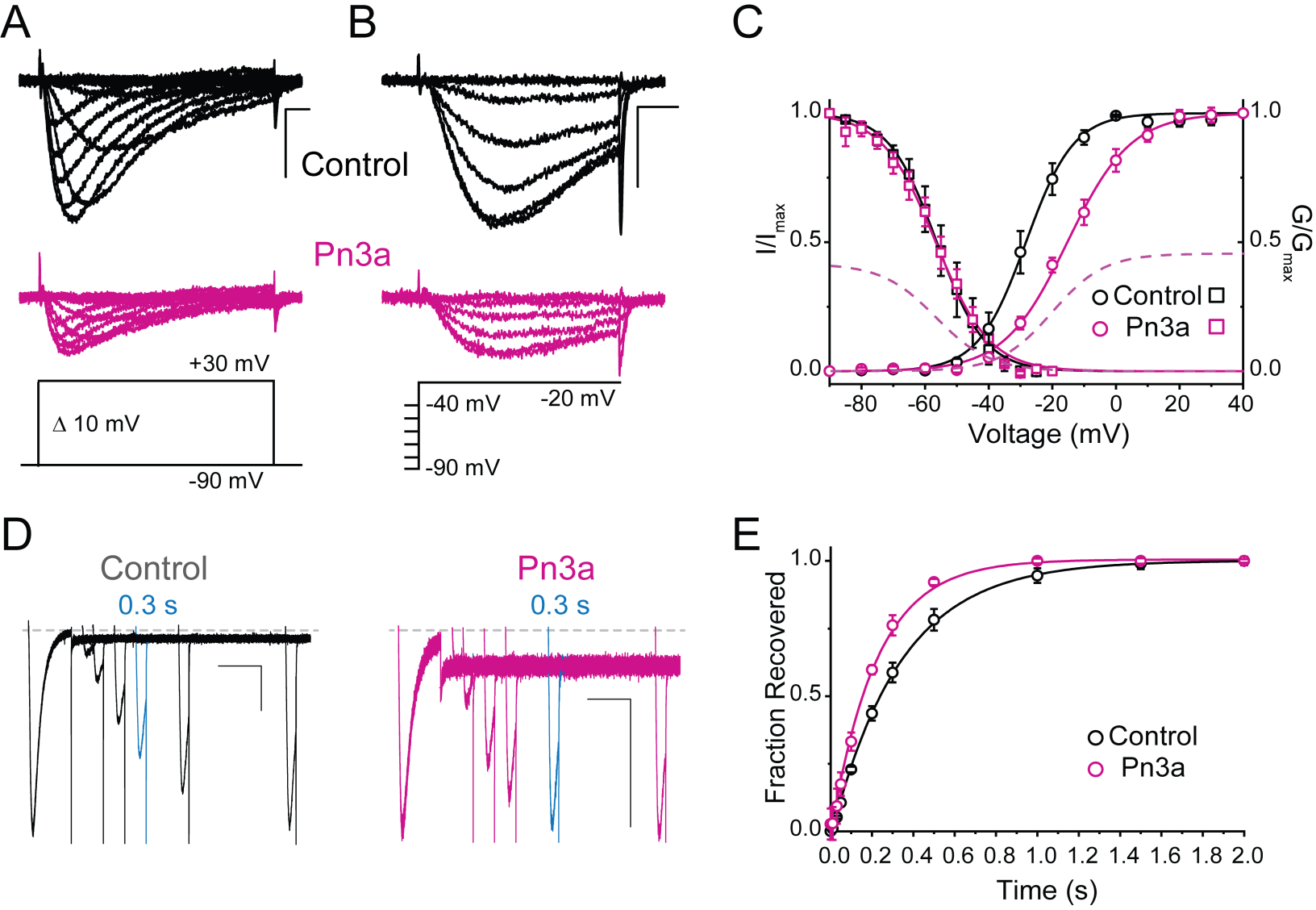
A
B
C
Control
Pn3a
+30 mV
Δ 10 mV
-90 mV
-40 mV
-20 mV
-90 mV
1.0
0.5
0.0
I/I max
G/G max
Control
Pn3a
-80
-60
-40
-20
0
20
40
Voltage (mV)
D
Control
0.3 s
Pn3a
0.3 s
E
Fraction Recovered
Control
Pn3a
0.0 0.2 0.4 0.6 0.8 1.0 1.2 1.4 1.6 1.8 2.0
Time (s)

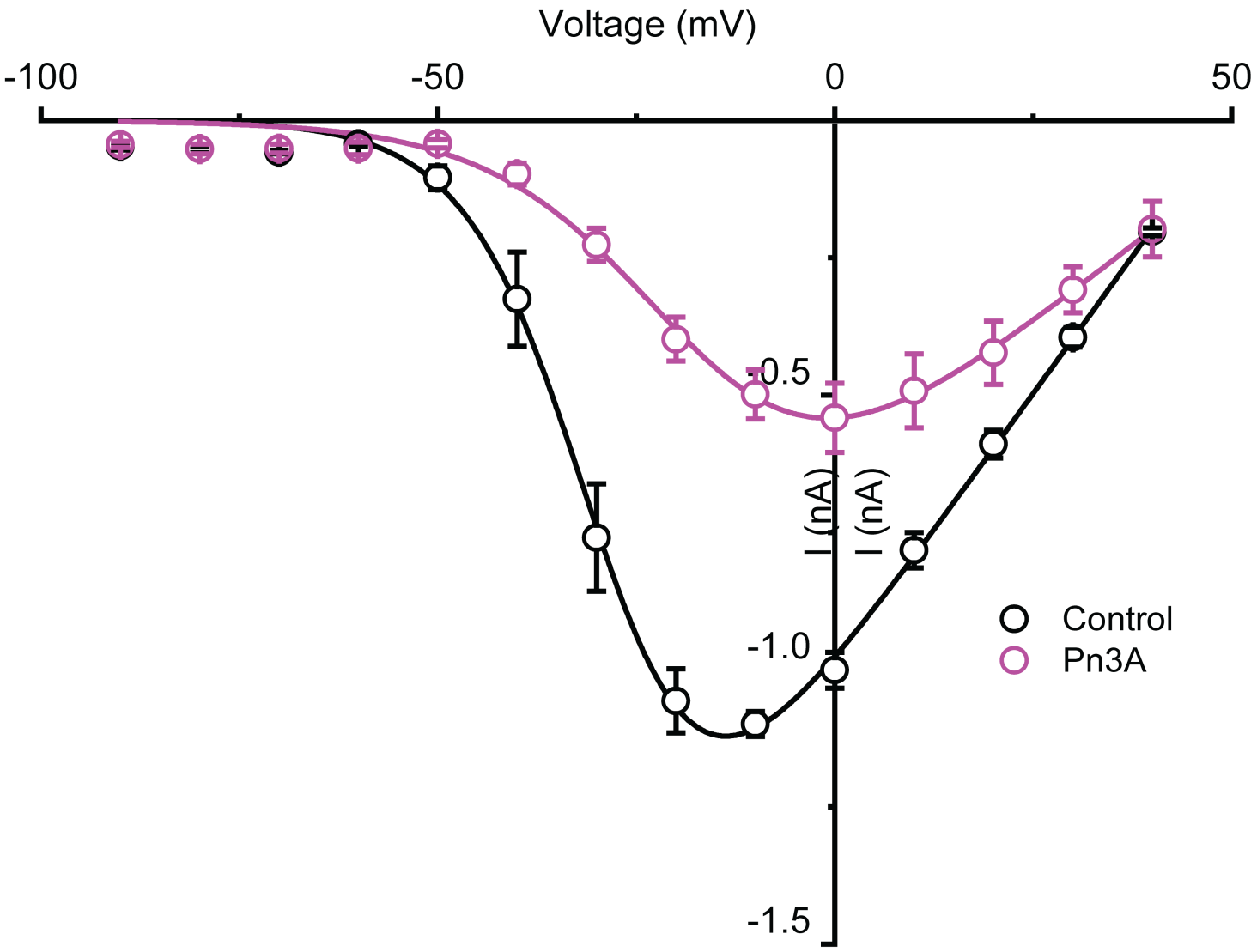
Voltage (mV)
-100
-50
0
50
-0.5
-1.0
-1.5
I (nA)
I (nA)
Control
Pn3A

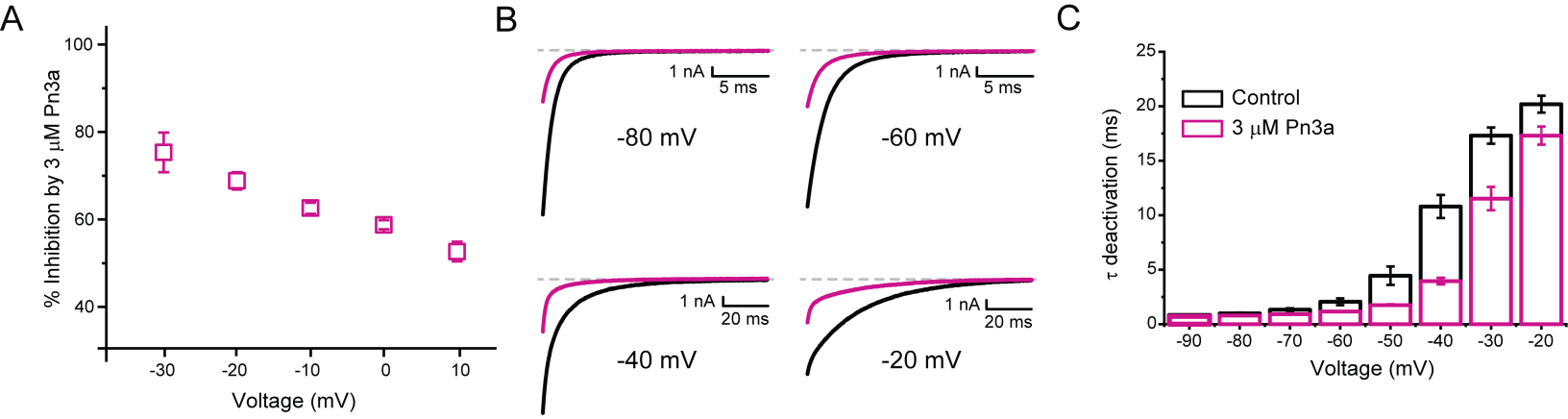
A
% Inhibition by 3 μM Pn3a
100
80
60
40
-30
-20
-10
0
10
Voltage (mV)
B
1 nA
5 ms
-80 mV
1 nA
5 ms
-60 mV
1 nA
20 ms
-40 mV
1 nA
20 ms
-20 mV
C
τ deactivation (ms)
25
20
15
10
5
0
Control
3 μM Pn3a
-90
-80
-70
-60
-50
-40
-30
-20
Voltage (mV)

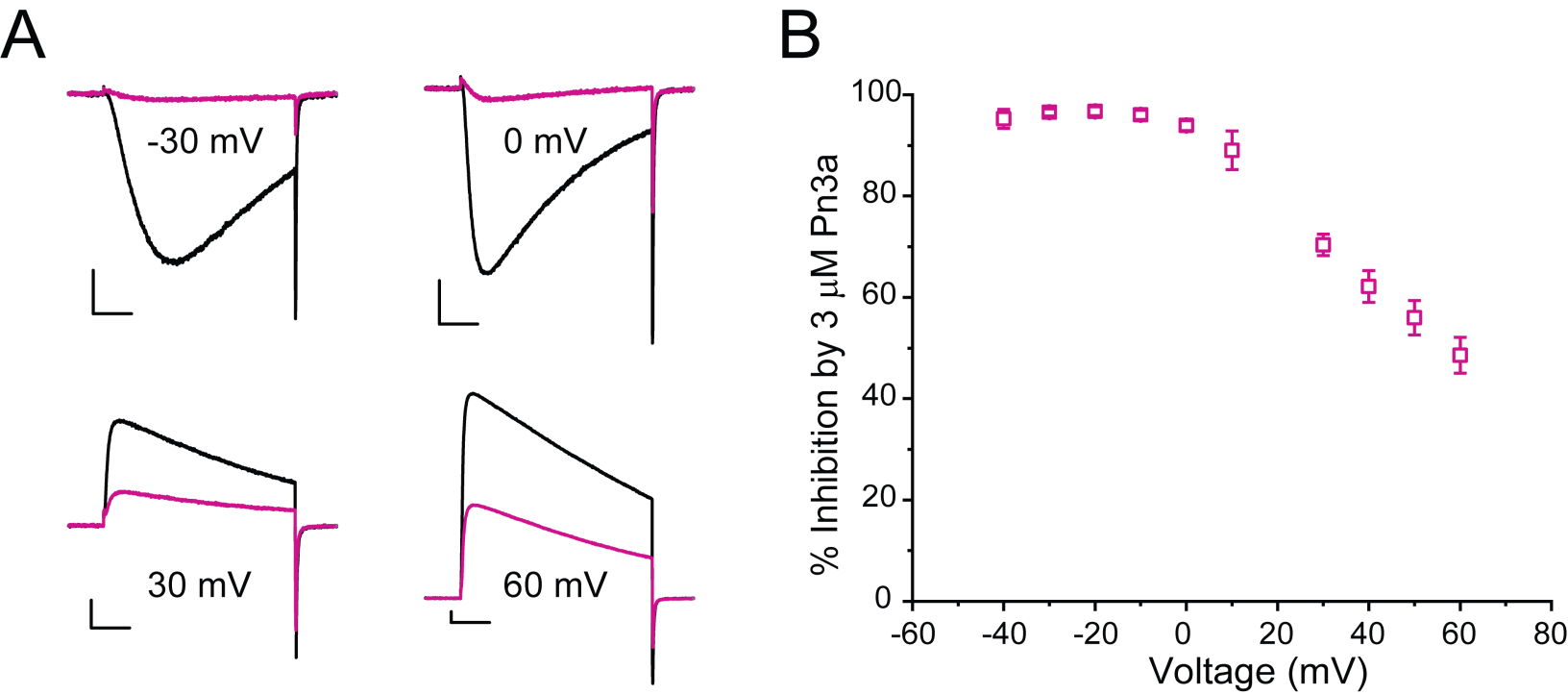
A
-30 mV
0 mV
30 mV
60 mV
B
% Inhibition by 3 μM Pn3a
100
80
60
40
20
0
-60
-40
-20
0
20
40
60
80
Voltage (mV)

A

S3b S4

```
Cav3.3 DI    NRLDFFIVMAGMVEYSLDLQNINLSAI--------RTVRVLRPLKAINRVPSMRI
Cav3.3 DII   NIFDSIIVIISIWEIVGQADGGLSVL---------RTFRLLRVLKLVRFMPALRR
Cav3.3 DIII  NVLDGFLVFVSIIDIVVSLASAGGAKILGVL----RVLRLLRTLRPLRVISRAPG
Cav3.3 DIV   NQLDLAIVLLSVMGITLEEIEINAALPINPTII--RIMRVLRIARVLKLLKMATG
Kv1.7        NLIDFVAILPYFVALGTELARQRGVGQQAMSLAILRVIRLVRVFRIFKLSRHSKG
```

B

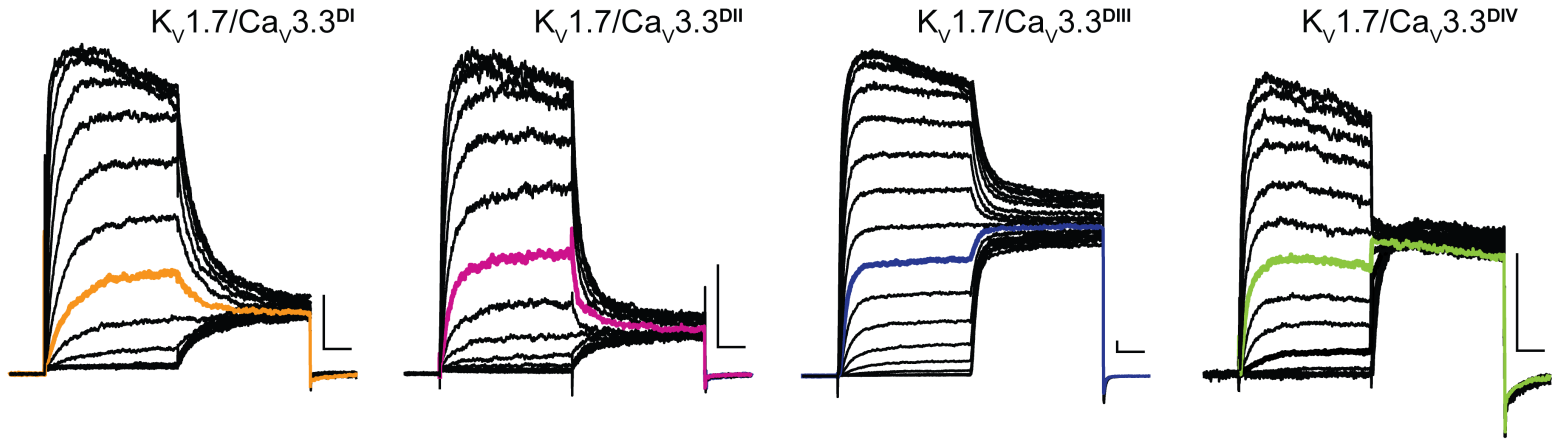

C

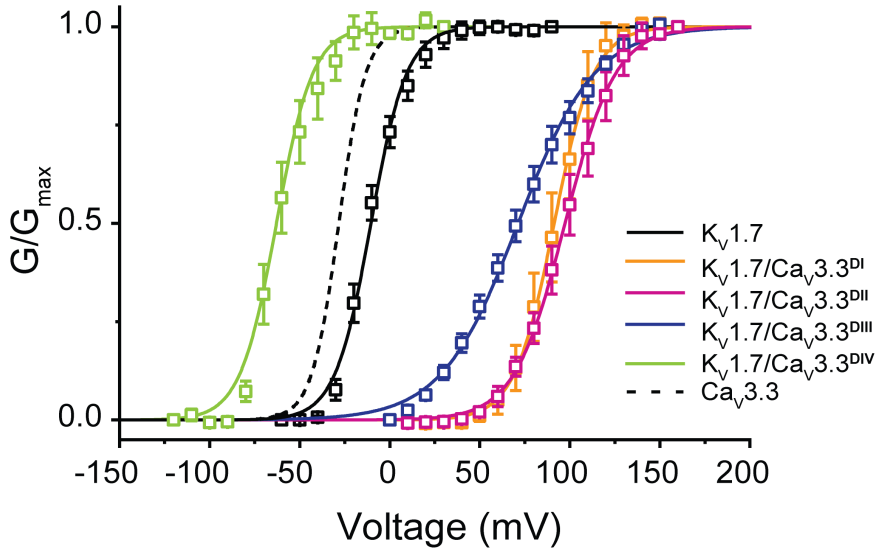

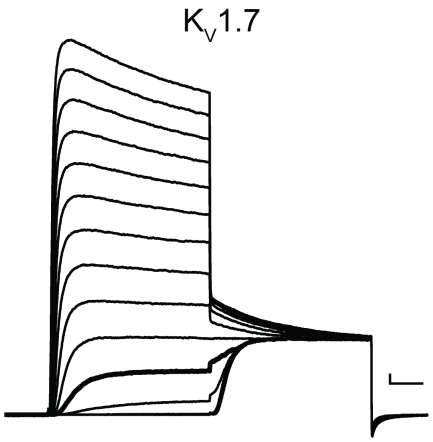

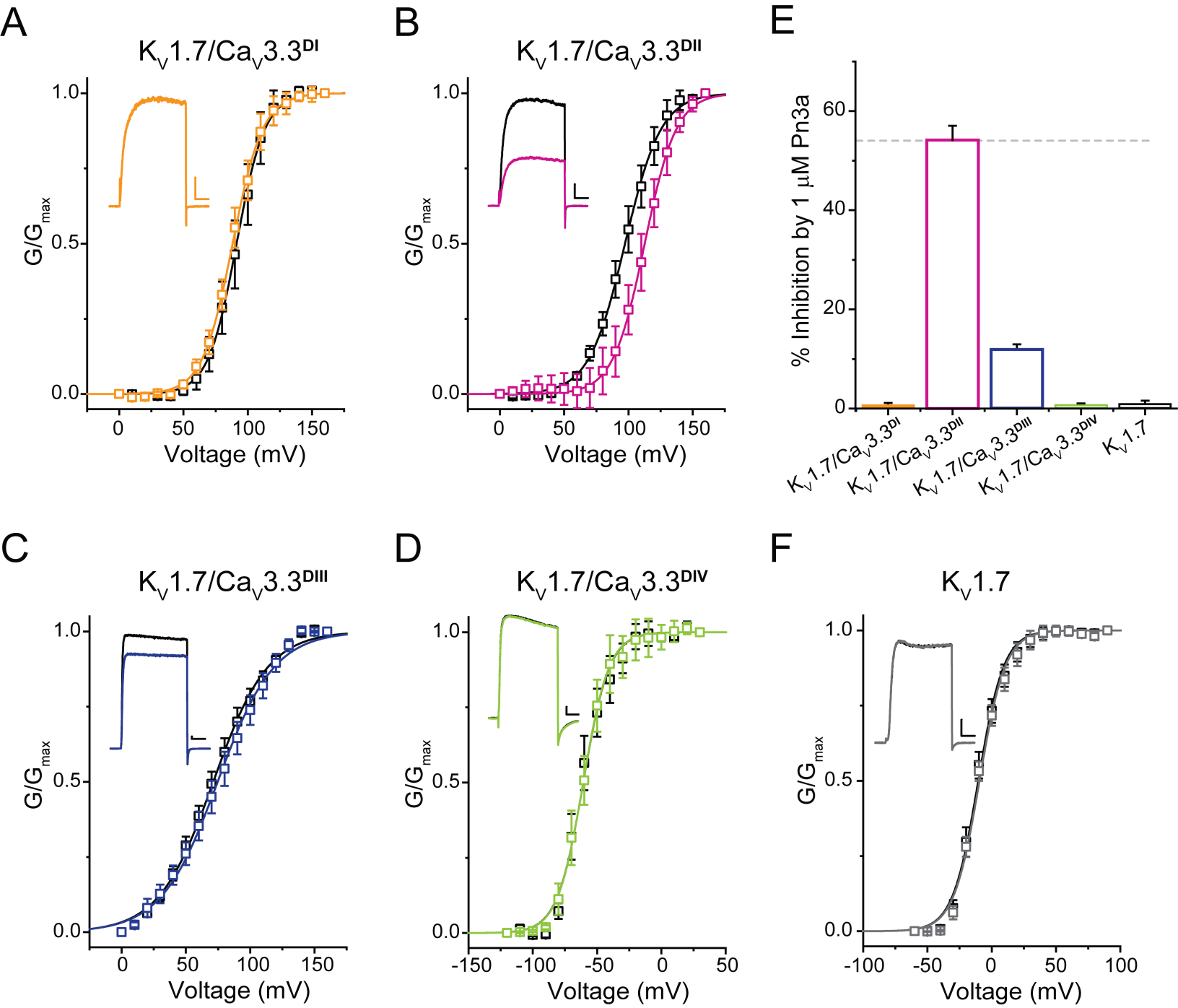
A
$K_V1.7/Ca_V3.3^{DI}$
B
$K_V1.7/Ca_V3.3^{DII}$
E
% Inhibition by 1 μM Pn3a
$K_V1.7/Ca_V3.3^{DI}$
$K_V1.7/Ca_V3.3^{DII}$
$K_V1.7/Ca_V3.3^{DIII}$
$K_V1.7/Ca_V3.3^{DIV}$
$K_V1.7$
C
$K_V1.7/Ca_V3.3^{DIII}$
D
$K_V1.7/Ca_V3.3^{DIV}$
F
$K_V1.7$
G/G_{max}
Voltage (mV)

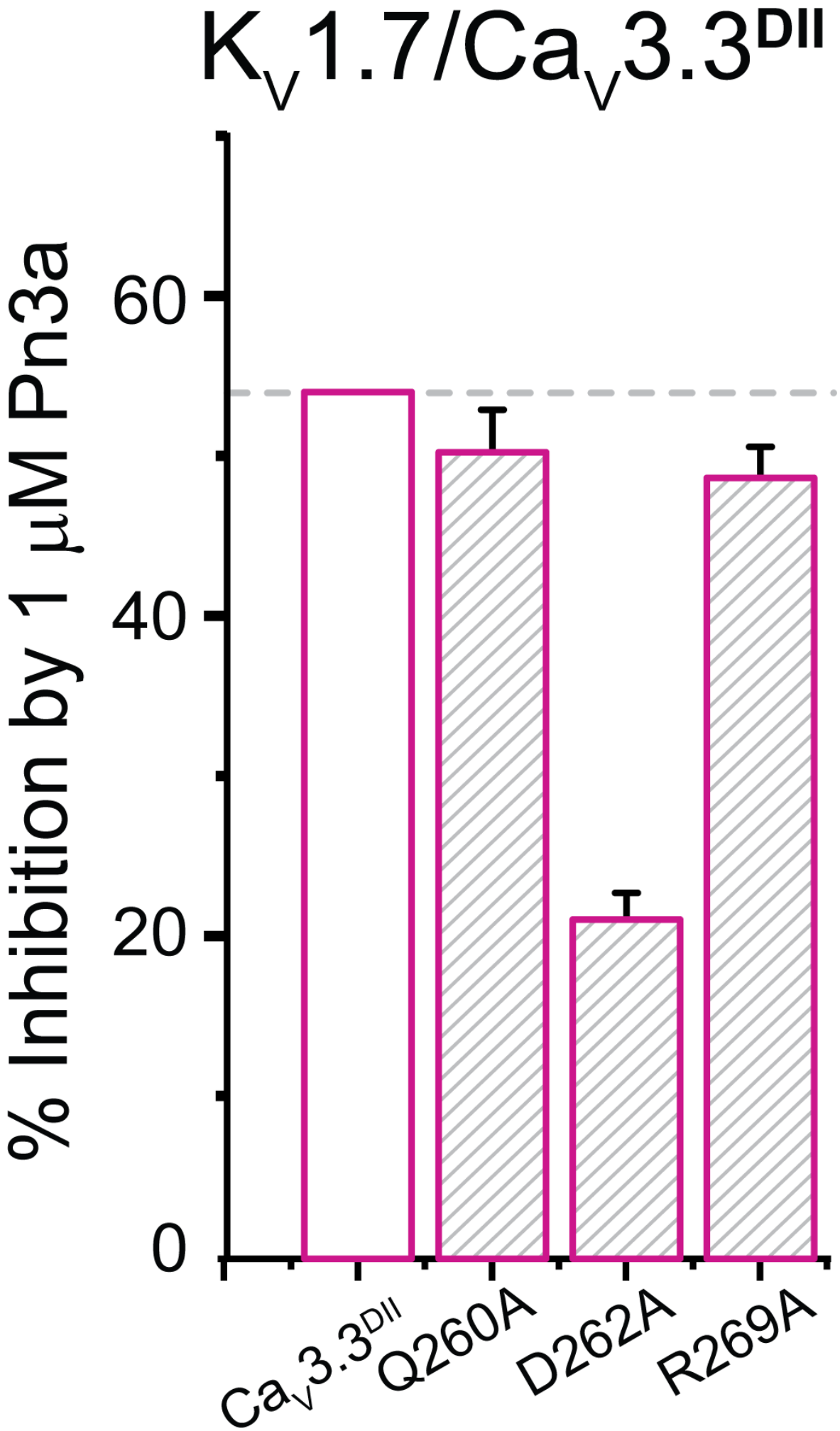
$K_V1.7/Ca_V3.3^{DII}$
% Inhibition by 1 µM Pn3a
60
40
20
0
$Ca_V3.3^{DII}$
Q260A
D262A
R269A

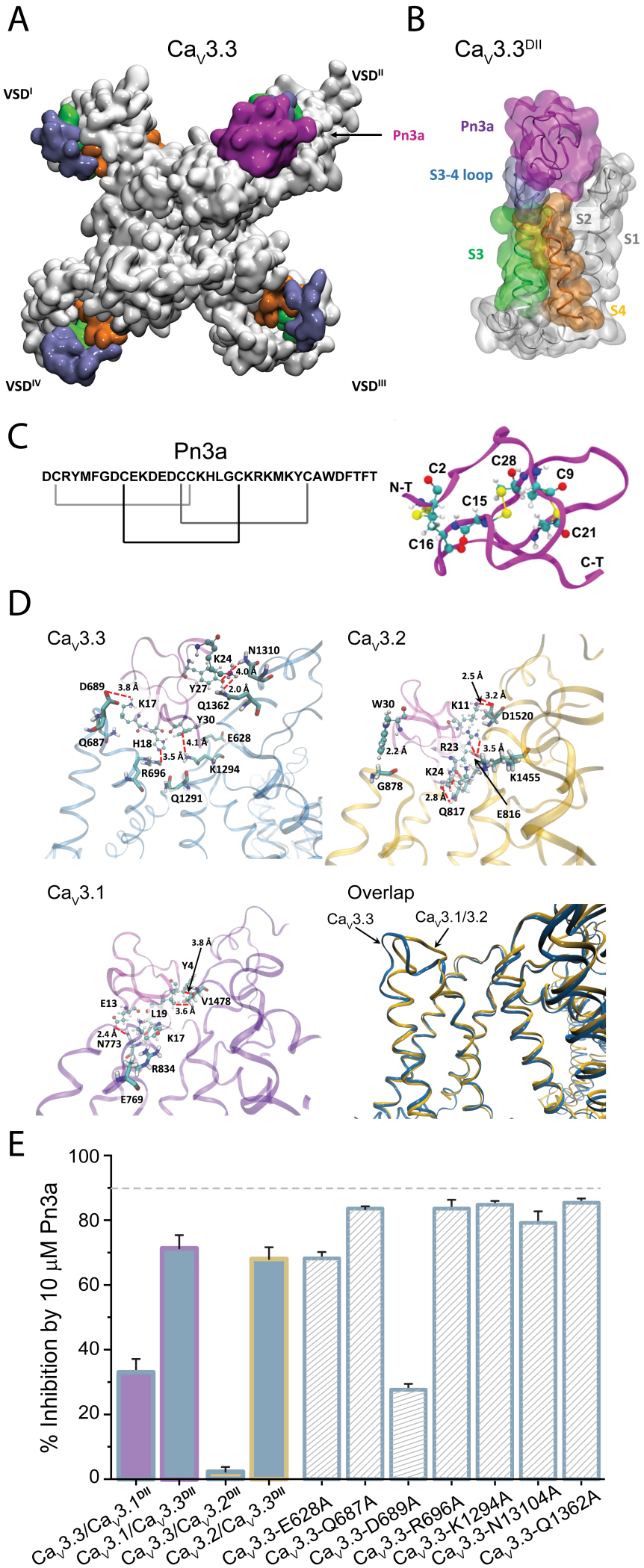
A
Ca$_V$3.3
VSD^I
VSD^{II}
Pn3a
VSD^{IV}
VSD^{III}
B
Ca$_V$3.3^{DII}
Pn3a
S3-4 loop
S2
S1
S3
S4
C
Pn3a
DCRYMFGDCEKDEDCCKHLGCKRKMKYCAWDFTFT
N-T
C2
C28
C9
C15
C16
C21
C-T
D
Ca$_V$3.3
N1310
K24
4.0 Å
D689
3.8 Å
K17
Y27
2.0 Å
Q1362
Y30
Q687
H18
4.1 Å
E628
3.5 Å
R696
K1294
Q1291
Ca$_V$3.2
2.5 Å
3.2 Å
W30
K11
D1520
2.2 Å
R23
3.5 Å
K24
K1455
G878
2.8 Å
Q817
E816
Ca$_V$3.1
3.8 Å
Y4
E13
V1478
L19
3.6 Å
2.4 Å
N773
K17
R834
E769
Overlap
Ca$_V$3.3
Ca$_V$3.1/3.2
E
% Inhibition by 10 μM Pn3a
100
80
60
40
20
0
Ca$_V$3.3/Ca$_V$3.1^{DII}
Ca$_V$3.1/Ca$_V$3.3^{DII}
Ca$_V$3.3/Ca$_V$3.2^{DII}
Ca$_V$3.2/Ca$_V$3.3^{DII}
Ca$_V$3.3-E628A
Ca$_V$3.3-Q687A
Ca$_V$3.3-D689A
Ca$_V$3.3-R696A
Ca$_V$3.3-K1294A
Ca$_V$3.3-N13104A
Ca$_V$3.3-Q1362A

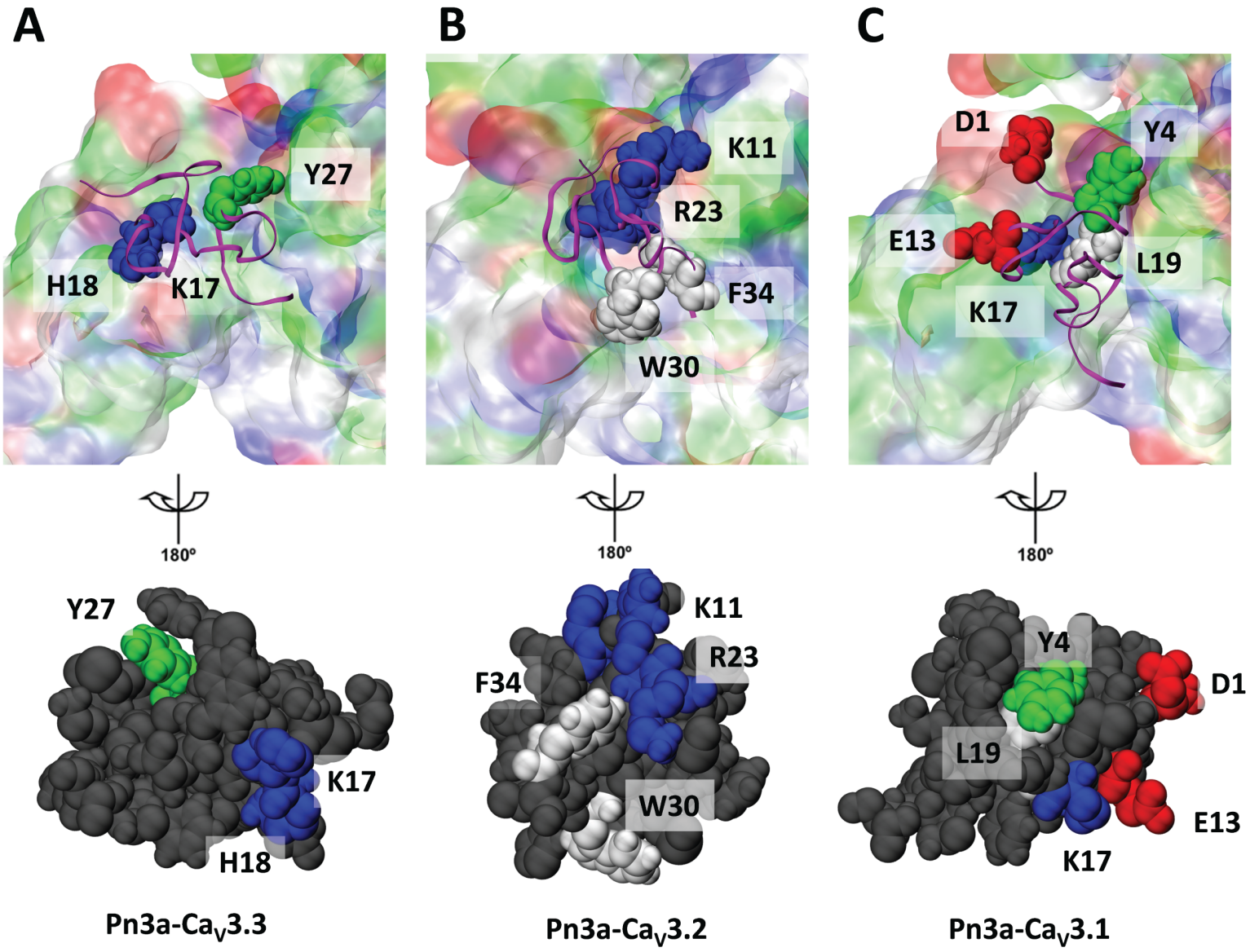
A
Y27
H18
K17
180°
Y27
K17
H18
Pn3a-Ca$_V$3.3
B
K11
R23
F34
W30
180°
K11
R23
F34
W30
Pn3a-Ca$_V$3.2
C
D1
Y4
E13
L19
K17
180°
Y4
D1
L19
E13
K17
Pn3a-Ca$_V$3.1

Residues of hCa$_V$3 channels / Residues of Pn3a	Ca$_V$3.3	Ca$_V$3.2	Ca$_V$3.1
D1	–	–	E769 (4.0 Å)*
Y4	T634 (2.3 Å) *	–	–
Y27	D1361 (2.8 Å)	–	–
W30	–	G878 (3.7 Å)***	–
D31	K1296 (2.7 Å)**	–	–
F32	S693 (3.6 Å) **	–	–
F34	–	K1455 (3.5 Å)**	–

* van der Waals interactions

** cation-π interactions

*** hydrophobic interactions

VS Module	Binding Affinity (kcal/mol)
DI	-12.3
DII	-13.5
DIII	-12.3
DIV	-15.1